EFFECT OF AQUEOUS EXTRACT OF *Persea americana* (AVOCADO) SEED ON ARSENIC TRIOXIDE-INDUCED KIDNEY DAMAGE IN ADULT WISTAR RATS.

BY

OLORUNTOBA OLASILE KOFOWOROLA

BMS2001050

DEPARTMENT OF ANATOMY

SCHOOL OF BASIC MEDICAL SCIENCES

COLLEGE OF MEDICAL SCIENCES

UNIVERSITY OF BENIN,

BENIN CITY, EDO STATE.

SUPERVISOR

DR. E. O. IMAFIDON

FEBRUARY, 2025.

EFFECT OF AQUEOUS EXTRACT OF *Persea americana* (AVOCADO) SEED ON ARSENIC TRIOXIDE-INDUCED KIDNEY DAMAGE IN ADULT WISTAR RATS.

BY

OLORUNTOBA OLASILE KOFOWOROLA

BMS2001050

DEPARTMENT OF ANATOMY

SCHOOL OF BASIC MEDICAL SCIENCES

COLLEGE OF MEDICAL SCIENCES

UNIVERSITY OF BENIN,

BENIN CITY, EDO STATE.

SUPERVISOR

DR. E. O. IMAFIDON

FEBRUARY, 2025.

DECLARATION

I declare that:

1. This project report is based on the experimental work undertaken by me in the Department of Anatomy, University of Benin, under the supervision of Dr. E. O. Imafidon.
2. This work has not been previously submitted for the award of a degree elsewhere.
3. All ideas and views are essentially based on this research. And where the views of others have been expressed, such words were duly acknowledged.

_____

OLORUNTOBA OLASILE KOFOWOROLA

CERTIFICATION OF PROJECT ON PLAGIARISM

We the undersigned attest that the project was undertaken by:

OLORUNTOBA OLASILE KOFOWOROLA

Titled:

EFFECT OF AQUEOUS EXTRACT OF Persea americana (AVOCADO) SEED ON ARSENIC TRIOXIDE-INDUCED KIDNEY DAMAGE IN ADULT WISTAR RATS.

Has successfully passed the anti-plagiarism test and does not violate any copyright regulations.

_____ _____

DR. E. O. IMAFIDON **DATE**

(SUPERVISOR)

_____ _____

DR. ADAZE BIJOU ENOIGERU **DATE**

(HEAD OF DEPARTMENT)

CERTIFICATION

This is to certify that this dissertation is the original work of **OLORUNTOBA OLASILE KOFOWOROLA** and has been approved in the Department of Anatomy, School of Basic Medical Sciences, College of Medical Sciences, University of Benin, Benin City, Edo State, Nigeria.

_____	_____
DR. E. O. IMAFIDON	**DATE**
(SUPERVISOR)	
_____	_____
ADAZE B. ENOGIERU (PHD)	**DATE**
(HEAD OF DEPARTMENT)	
_____	_____
EXTERNAL EXAMINER	**DATE**

DEDICATION

This project is dedicated to God Almighty and to the Department of Anatomy, School of Basic Medical Sciences.

ACKNOWLEDGMENT

I would like to express my deepest gratitude to my parents (Elder and Deaconess Oloruntoba) for their invaluable guidance, unwavering support financially and emotionally, and continuous encouragement throughout this project.

My deepest appreciation goes to my esteemed supervisor DR. E. O. Imafidon of the department of Anatomy, School of Basic Medical Sciences, University of Benin, for his patience, guidance and intellectual inputs that were really helpful to me till the project's completion. The completion of the project would not have been possible without his corrections and insights which he took time from his busy schedule to attend to. May God almighty bless you abundantly in all areas of your life.

I extend my appreciation to my supportive siblings; Agboola Glory, Kingsley, and Loveth, my colleagues and friends; Ale Oluwagbenga, Deniran Lysa, Ejiakhila Amelia, Ebuka Okongwu, Abizu Emmanuella, Divine and others not mentioned, for their support which was a source of strength and motivation during the course of this project.

I would like to extend my gratitude to the Masters Students and staffs of the Department of Anatomy, School of Basic Medical Sciences, Mr Raymond, Mr Sam and Mr John for their intellectual support and counsel.

TABLE OF CONTENTS

LIST OF PLATES

ABSTRACT

Environmental toxicants, such as arsenic, pose significant health risks, particularly to vital organs like the kidneys. As key organs responsible for filtration and detoxification, the kidneys are especially vulnerable to the oxidative stress and inflammation caused by arsenic exposure.

Inorganic arsenic, a highly toxic form found in contaminated water, food, and soil, accumulates in kidney tissues, leading to cellular damage, impaired function, and an increased risk of chronic kidney disease and other renal disorders. The generation of reactive oxygen species (ROS) by arsenic, disrupts cellular homeostasis, damages mitochondrial function, and triggers pro-inflammatory responses, exacerbating kidney injury.

Nutrient-rich foods like *Persea americana* offer a potential protective strategy against arsenic-induced kidney damage. *Persea americana* are abundant in antioxidants, phenolic compounds, and unsaturated fatty acids that combat oxidative stress, reduce inflammation, and enhance cellular resilience. These bioactive compounds help neutralize ROS, improve mitochondrial function, and mitigate arsenic's toxic effects on kidney tissues, supporting overall renal health and function.

Accordingly, this study aimed to investigate the effect of aqueous extract of *Persea americana* on arsenic-induced kidney damage in fully-grown Wistar rats. Thirty (30) fully-grown Wistar rats were used weighing between 130g and 150g. They were grouped into six groups (A, B, C, D, E, and F). The rats in Group A served as the control, and the rats in Group B were administered 10mg/kg of Arsenic Trioxide, the rats in Group C were administered 140mg/kg body weight of Silymarin and 10mg/kg of arsenic trioxide, the rats in Group D were administered with 125mg/kg of *Persea americana* and 10mg/kg of arsenic trioxide, the rats in Group E were administered with 250mg/kg of *Persea americana* and 10mg/kg of arsenic trioxide and the rats

in Group F were administered with 10mg/kg of arsenic trioxide for 14 days and allowed to recover. The administration period spanned 28 days after which they were sacrificed and the kidneys harvested were collected for biochemical and histological assessments. Results showed no significant difference ($p>0.05$) in the kidney weight, and Reno-somatic index across the experimental groups, there was a significant decrease in the weight of the group treated with 10mg/kg of arsenic trioxide compared to the control group. In the case of the oxidative stress parameters arsenic, caused a is significant decrease in SOD, and GPX activities and a significant increase in MDA activities when compared with control while treatment group was able to reverse these significant changes except for the recovery group. For the urea and creatinine level, there was a significant increase in the groups given 10mg/kg of arsenic trioxide and the group that was given 10mg/kg of arsenic trioxide and left to recover. The other groups had no significant difference in the urea and creatinine level when compared to the control group. In conclusion, this study suggests that *Persea americana* provides protection against arsenic trioxide-induced nephrotoxicity in Wistar rats.

CHAPTER ONE

INTRODUCTION

1.1 BACKGROUND OF THE STUDY

Heavy metals, herbicides, and industrial chemicals are among the environmental contaminants that greatly contribute to organ damage. The kidneys, which are essential for detoxification and waste removal, are especially affected (Tahir and Alkheraije, 2023). Arsenic among these toxicants is particularly harmful to renal function (Tahir and Alkheraije, 2023; Khalaf et al., 2024). This toxin is found in many different forms, including inorganic forms such as arsenic trioxide. It is typically exposed through contaminated food, drinking water, and industrial processes (Tahir and Alkheraije, 2023).

The nephrotoxic effects of arsenic trioxide are well known; after absorption, it builds up in kidney tissues, causing cellular disruption and serious damage (Su et al., 2023; Ganie et al., 2024). Its toxicity is mainly caused by the production of reactive oxygen species (ROS), which cause oxidative stress and damage essential cellular components like lipids, proteins, and DNA (Ganie et al., 2024). This oxidative damage impairs kidney function and encourages cell death. Moreover, arsenic trioxide disrupts mitochondrial activity, lowering energy production while raising ROS levels, aggravating renal damage (Su et al., 2023).

Arsenic trioxide's effect on kidney cells' calcium signaling is another important consequence. It causes enzymatic disruption and cellular malfunction and death by raising intracellular calcium levels (Su et al., 2023; Ganie et al., 2024). Additionally, arsenic trioxide aggravates tissue damage by triggering inflammatory mediators and immunological responses that cause inflammation in renal tissues (Ganie et al., 2024). These processes play a role in renal diseases like chronic kidney disease, fibrosis, and nephritis (Su et al., 2023; Ganie et al., 2024). By

strengthening the body's antioxidant defenses, arsenic trioxide-induced nephrotoxicity can be reduced.

A fruit known for its nutritional and therapeutic qualities, the *Persea americana* (avocado pear) may be able to prevent kidney damage brought on by arsenic. By neutralizing ROS and maintaining renal cell integrity, *P. americana*, which is abundant in antioxidants such polyphenols, flavonoids, and vitamin E, fights oxidative stress (Chinedu et al., 2021; Bangar et al., 2022). It has been demonstrated that P. americana's bioactive components improve kidney resilience to oxidative insults by lowering inflammation, repairing cellular damage, and stabilizing mitochondrial activity (Akusu et al., 2021; Bangar et al., 2022). A possible natural treatment for preventing arsenic trioxide-induced nephrotoxicity, preliminary research indicates that P. americana may reduce the formation of ROS, promote the production of mitochondrial energy, and reduce inflammatory responses (Omodamiro et al., 2021; Chinedu et al., 2021; Akusu et al., 2021; Bangar et al., 2022). By bolstering antioxidant defenses and reducing oxidative stress, *P. americana* provides a protective shield for the kidneys, highlighting its potential as an effective therapeutic agent in countering arsenic trioxide's toxic effects.

1.2 STATEMENT OF RESEARCH PROBLEM

Arsenic and its compounds are widely recognized as environmental contaminants with significant health implications, particularly affecting the kidneys. Arsenic is naturally found in the Earth's crust and commonly occurs in combination with other elements such as oxygen, chlorine, and sulfur rather than in its elemental form (Rae, 2020). This metalloid is known for its toxic effects on living organisms, particularly its ability to disrupt cellular and metabolic processes in vital organs, including the kidneys (Rae, 2020; Khan and Flora, 2023). Chronic

arsenic exposure has been linked to nephrotoxicity, with mechanisms involving oxidative stress, inflammation, and the impairment of cellular repair pathways (Derouiche et al., 2020).

Human exposure to arsenic primarily occurs through contaminated drinking water, food sources, and occupational hazards. In regions with significant arsenic contamination, such as areas relying on groundwater with naturally high arsenic levels or those impacted by industrial activities, the prevalence of kidney-related health issues has been documented (Palma-Lara et al., 2020). Studies have highlighted the presence of arsenic in water supplies exceeding the World Health Organization (WHO) guideline of 10 μg/L in several regions, with concentrations as high as 50 μg/L reported in certain areas (Rahman et al., 2013; Sorg et al., 2014). Similarly, food sources such as rice, which can accumulate arsenic from contaminated water and soil, have been shown to contribute significantly to dietary arsenic intake (Sharma et al., 2014).

In Nigeria, increasing arsenic exposure has emerged as a public health concern. Factors such as mining activities, pesticide use, and industrial emissions contribute to environmental arsenic contamination (Nweke and Sanders, 2009; Egbueri et al., 2024). For instance, a 2020 study by Emenike et al. (2019) revealed that arsenic concentrations in Nigerian groundwater often exceeded the WHO guideline, with mean levels of 20 μg/L reported in some areas. Another study detected elevated arsenic levels in crops irrigated with contaminated water, posing risks for chronic exposure and kidney-related complications (Onakpa et al., 2018). The evidence underscores the significant public health challenge posed by arsenic exposure in Nigeria, particularly concerning renal health. Addressing this issue requires urgent measures.

1.3 AIM AND SPECIFIC OBJECTIVES OF THE STUDY

The aim of the study was to investigate the effect of aqueous *Persea Americana* seed extract on arsenic trioxide-induced nephrotoxicity in adult Wistar rats.

The specific objectives of this study were to investigate the effects of aqueous extract of *Persea americana* seed on the:

- Kidney and body weight changes in adult Wistar rats.
- Oxidative stress parameters (superoxide dismutase, glutathione peroxidase, Malondialdehyde) in adult Wistar rats.
- Urea and Creatinine levels in adult Wistar rats
- Histology of the Kidney in adult Wistar rats

1.4 JUSTIFICATION OF THE STUDY

The rise in kidney disorders linked to environmental toxins highlights the urgent need for protective measures. Arsenic trioxide, a toxic industrial compound, is a key driver of nephrotoxicity, causing oxidative stress, inflammation and apoptosis (Liu et al., 2020; Jin et al., 2020). These processes damage renal tissues and disrupt kidney function, which is vital for detoxification and homeostasis.

Persea americana, a medicinal plant rich in antioxidants, has been suggested to exhibit nephroprotective potential (Yusuf et al., 2023). It is believed to scavenge free radicals, reduce oxidative stress, and influence cellular processes critical to maintaining renal function and cell survival (Yusuf et al., 2023; Okoduwa, 2024). Some studies have explored its protective effects in various nephrotoxic conditions, including drug-induced nephrotoxicity, heavy metal toxicity, and ischemia-reperfusion injury. However, there is a dearth of information on the role of *Persea americana* in mitigating arsenic trioxide-induced nephrotoxicity.

CHAPTER TWO

LITERATURE REVIEW

2.1 PLANT OF STUDY: *Persea americana* seed

2.1.1 Description and Scientific Classification

Avocado trees can grow tall or develop a broad, spreading canopy, with elliptic to egg-shaped leaves measuring 10 to 30 cm (4 to 12 inches) long. Their small, greenish flowers cluster densely, lacking true petals and featuring nine stamens in three series, along with a single-celled ovary (Ochoa-Zarzosa et al., 2021). Avocado flowers are classified into two types, A and B, which exhibit dichogamy, meaning their male and female parts mature at different times.

Fig. 2.1: *P. americana* fruit and seed (Márquez-Santos et al., 2020)

Type A flowers are functionally female in the morning, close by midday, and reopen as functionally male the next afternoon, while Type B flowers are female in the afternoon, close by evening, and reopen as male the following morning. Growing both types together enhances cross-pollination and fruit yield (Márquez-Santos et al., 2020; Subhagan et al., 2020). The size, shape, and color of avocado fruit vary widely by variety. Some Mexican avocados can be as small as a hen's egg, while others weigh between 1 and 2 kg (2 to 4 pounds) (Hurtado-Fernández et al., 2018). The fruit can be round or pear-shaped, sometimes with a long neck, and its skin color ranges from green to dark purple (Ochoa-Zarzosa et al., 2021). Classified botanically as a berry, the avocado contains a large seed surrounded by two cotyledons, with outer skin that can be thin and smooth, like an apple, or coarse and woody.

Scientific Classification:

Kingdom: Plantae

Clade: Tracheophytes

Clade: Angiosperms

Clade: Magnoliids

Order: Laurales

Family: Lauraceae

Genus: *Persea*

Species: *P. americana*

2.1.2 Phytochemical Constituents

Persea americana have been widely used in traditional medicine due to their reported therapeutic effects on hyperlipidemia, hypertension, and hypercholesterolemia. Setyawan *et al.*

(2021) explored the chemical composition of avocado seed extracts prepared using hexane, acetone, ethanol, and water through qualitative and quantitative analyses. The qualitative analysis revealed that hexane extracts contained fatty acids, while acetone extracts included fatty acids, phenols, tannins, and flavonoids. Ethanol extracts were found to contain phenols, tannins, flavonoids, and alkaloids, whereas water extracts contained carbohydrates, phenols, and tannins. Bangar *et al.* (2022) conducted quantitative analysis using gravimetric methods for alkaloids and ultraviolet spectrophotometry for flavonoids, phenols, and tannins. Results indicated that the ethanol extract had an alkaloid content of 0.435%, while the acetone and ethanol extracts contained flavonoids at levels of 0.1068% and 0.1084%, respectively. The phenol content in the acetone, ethanol, and water extracts was 0.0476%, 0.0309%, and 0.0494%, respectively, while the tannin content in acetone, ethanol, and water extracts was 0.1989%, 0.2044%, and 0.1804%, respectively (Bangar et al., 2022).

In a related study by Akusu et al. (2021), the chemical composition of *Persea americana* leaf extracts prepared using hexane, acetone, ethanol, and water was also examined. The extraction process employed maceration for hexane, acetone, and ethanol solvents and an infusion method for water. Qualitative analysis showed that hexane extracts contained flavonoids and alkaloids, acetone extracts contained flavonoids, phenols, tannins, and alkaloids, ethanol extracts contained flavonoids, phenols, tannins, alkaloids, and saponins, and water extracts contained flavonoids, phenols, tannins, and alkaloids.

Quantitative analysis revealed that flavonoid levels in hexane, acetone, ethanol, and water extracts were 0.6%, 0.3%, 0.3%, and 0.5%, respectively, while phenol levels in acetone, ethanol, and water extracts were 5.1%, 3.9%, and 3.7%, respectively. Tannin levels in acetone, ethanol, and water extracts were 0.3%, 0.2%, and 0.1%, respectively. Alkaloid levels in hexane, acetone,

ethanol, and water extracts were 0.1%, 13.6%, 15.6%, and 5.5%, respectively, and the ethanol extract contained 3.3% Saponins (Akusu et al., 2021; Chinedu et al., 2021). These findings provide valuable insights into the diverse chemical constituents present in both avocado seeds and leaves, highlighting their potential therapeutic and pharmaceutical applications (Chinedu et al., 2021).

2.1.3 Pharmacological Activities

2.1.3.1 Vasorelaxant activity

Researchers have reported that avocado leaf extract exerts vasorelaxant effects on isolated rat aorta by stimulating the release of endothelium-derived relaxing factors (EDRFs) and prostanoids. Additionally, treatment with the extract reduces vasoconstriction by inhibiting the influx of calcium ions (Ca^{2+}) (Omodamiro et al., 2021; Demirel, 2024).

2.1.3.2 Anti-Inflammatory activity

Prostaglandins and leukotrienes, derived from arachidonic acid through the actions of cyclo-oxygenase and lipoxygenase enzymes, are key members of the eicosanoid family [8,9]. Eicosanoids play a crucial role in both physiology and pathology, particularly as mediators of inflammation (Dabas et al., 2019; Ndidiamaka et al., 2023).

Avocado seeds have demonstrated anti-inflammatory properties, partly due to their ability to modulate enzymatic activity. Phospholipase A2 (PLA2), a critical enzyme in inflammation, releases arachidonic acid from membrane phospholipids. Compounds such as lipidic polyols, isolated from avocado seeds, have been shown to inhibit PLA2 activity, thereby contributing to their anti-inflammatory effects.

2.1.3.3 Hypotensive potential

Avocado (*Persea americana*) seed extract is commonly used in Nigeria for managing hypertension. Studies have demonstrated its efficacy in reducing blood pressure and improving related metabolic parameters. In one study, an aqueous seed extract from Fuerte avocados, administered at doses of 200–600 mg/kg body weight (bw), significantly lowered blood pressure in NaCl-induced hypertensive rats after four weeks of treatment. This was accompanied by reductions in plasma triglycerides (TG), total serum cholesterol (TC), and low-density lipoprotein cholesterol (LDL-C) at doses of 500 mg/kg bw and above (Omodamiro et al., 2021). Similarly, another study showed that a 200–600 mg/kg bw dose of aqueous avocado seed extract reduced blood pressure, cholesterol, glucose, urea, and sodium levels in hypertensive rats in a dose-dependent manner over five weeks (Assoumou et al., 2021). Additionally, acute treatment of acetylcholine-induced hypertensive rats with an aqueous seed extract at 260 mg/kg bw for 10 days resulted in significant reductions in mean arterial pressure (37–43%) and heart rate (9.3–19.7%) (Sokpe et al., 2020; Omodamiro et al., 2021).

2.1.3.4 Anticonvulsant activity

Aqueous extract of *Persea americana* (P. americana) leaves has demonstrated anticonvulsant effects in mice (Omodamiro et al., 2021). The effectiveness of the plant extract in the experimental convulsion model suggests its potential for treating both petit mal and grand mal epilepsy.

Convulsions induced by pentylenetetrazol (PTZ) and picrotoxin (PCT) were more effectively mitigated by the leaf extract compared to seizures induced by bicuculline (BCL) (Omodamiro et al., 2021). Notably, the onset of convulsions was significantly delayed, and their duration was markedly shortened. These findings suggest that the aqueous extract of *P. americana* leaves may

reduce susceptibility to PTZ, PCT, and BCL-induced seizures, possibly by enhancing or inhibiting GABAergic activity and/or neurotransmission in the brain (Egbuonu et al., 2018; Omodamiro et al., 2021).

2.1.3.5 Antioxidant activity

Avocado oil has antioxidant activity by reducing the formation of ROS in the damaged mitochondria. Based on the data that avocado oil favourably changed hepatic indicators in rats given sugar, which had altered hepatic markers, it has been claimed that avocado oil is an effective dietary supplement for managing metabolic diseases. Additionally, it promotes liver regeneration (Sunday et al., 2022).

2.1.3.6 Antidiabetic activity

In laboratory models, avocado seed extracts have been demonstrated to lower blood sugar and improve diabetes. Experimentally, it has been found that 14-day treatment with ethanolic seed extract (450 or 900 mg/kg bw) to lower blood glucose levels by 47 to 55% In Alloxan-induced diabetic. Histopathological studies indicated that the extract has protective effect on pancreatic islet cells (Umoh et al., 2019).

Ebifa et al. (2021) discovered that treatment with aqueous seed extract (300 or 600mg/kg bw) for 21 days decreased plasma glucose concentrations by 73 and 78%, respectively. The presence of insulin-mimetic compounds in the extract, which promote insulin secretion by B cells or improve glucose utilisation, is thought to be the cause of the extract's hypoglycaemic effects.

2.1.3.7 Anticancer activity

The anticancer properties of avocado seed and peel extracts have primarily been attributed to their activation of caspase-3, caspase-7, and the cleavage of poly (ADP ribose) polymerase. Additionally, studies have shown that treatment with methanolic extract from avocado seed (100

μg/ml) induces apoptosis in MDA-MB-231 human breast cancer cells. Notably, compared to the seeds, the peel contains higher levels of total phenolic compounds and total flavonoids (Ahmed et al., 2022).

2.2 ARSENIC TRIOXIDE

Arsenic trioxide (As_2O_3) is a white, odorless powder with low aqueous solubility, primarily produced as a by-product of metal smelting (Gill, 2024). Historically, arsenic compounds have been used in medicine, including as a treatment for acute promyelocytic leukemia. Arsenic exposure, mainly through contaminated water, food, or inhalation in occupational settings, poses serious health risks, including cancer, cardiovascular disease, diabetes, and chronic kidney disease. Arsenic is also used in semiconductors, pesticides, and animal feed (Bagga and Chawla, 2025).

2.2.1 Toxicokinetics

Arsenic toxicity disrupts cellular energy pathways, DNA replication, and repair by inactivating enzymes and substituting phosphate in high-energy compounds like ATP. It generates reactive oxygen species, causing lipid peroxidation and DNA damage. Arsenite binds to thiol groups in proteins across organs such as the liver, lungs, and kidneys, as well as in keratin-rich tissues like skin and nails (Gill, 2024; Bagga and Chawla, 2025).

2.2.1.1 Absorption

Arsenic trioxide is absorbed predominantly in the small intestine through an electrogenic process facilitated by a proton (H^+) gradient (El-Ghiaty et al., 2022). The optimal pH for this absorption is approximately 5.0; however, the small bowel environment, influenced by pancreatic bicarbonate secretion, generally maintains a pH closer to 7.0 (El-Ghiaty et al., 2022; Gill, 2024). Arsenic absorption can also occur via inhalation when particulate arsenic is deposited in the

alveoli of the lungs, where it enters systemic circulation. Dermal absorption is minimal under normal conditions, but prolonged or repeated skin exposure to arsenic compounds can lead to systemic entry (El-Ghiaty et al., 2022).

2.2.1.2 Distribution

Once absorbed, arsenic is quickly transported via the bloodstream to various tissues. In the initial phase, it accumulates in metabolically active organs, including the liver, kidneys, and lungs, where it exerts toxic effects. Over time and with chronic exposure, arsenic accumulates in keratin-rich tissues such as the hair, nails, and skin (Madrigal-Redondo et al., 2023). Additional long-term storage occurs in the liver, kidneys, heart, and lungs, leading to progressive tissue damage. Arsenic binds strongly to thiol or sulfhydryl groups in proteins, disrupting normal cellular functions. Furthermore, arsenic has the ability to cross the placenta, posing a significant risk to fetal development by interfering with embryonic cellular pathways (El-Ghiaty et al., 2022; Madrigal-Redondo et al., 2023).

2.2.1.3 Metabolism

Metabolism of arsenic primarily takes place in the liver, where it undergoes sequential methylation to produce monomethylarsonic acid (MMA) and dimethylarsinic acid (DMA). These methylated metabolites are less toxic than their inorganic precursors but are not entirely innocuous (Ahmad and Khan, 2023). The methylation process is mediated by arsenic methyltransferase (AS_3MT) and relies on S-adenosylmethionine (SAM) as a methyl donor. Incomplete methylation or individual variability in methylation efficiency can lead to higher retention of toxic inorganic arsenic species (Ahmad and Khan, 2023; Gill, 2024). Metabolic processing of arsenic is also associated with the generation of reactive oxygen species (ROS),

which contribute to oxidative stress, cellular lipid peroxidation, and DNA damage, further exacerbating its toxic effects (Gill, 2024).

2.2.1.4 Excretion

The primary route of arsenic excretion is through the urine. Approximately 50% of the absorbed arsenic dose is eliminated within 3–5 days, primarily in the form of dimethylarsinic acid (60%–70%) and monomethylarsonic acid, with a smaller fraction of unchanged inorganic arsenic (Chen and Costa, 2021). While urinary excretion is the main pathway, fecal elimination contributes minimally to arsenic clearance. In cases of chronic exposure, residual arsenic persists in keratin-rich tissues, including hair and nails, which serve as biomarkers for prolonged exposure and can remain detectable for weeks or months after ingestion (Chen and Costa, 2021; Ahmad and Khan, 2023).

2.2.1.5 Storage and Accumulation

During acute arsenic poisoning, the highest concentrations of arsenic are found in the kidneys and liver, as these organs play pivotal roles in arsenic metabolism and excretion. Chronic exposure leads to widespread accumulation in multiple organs, including the liver, kidneys, heart, and lungs, as well as the gastrointestinal tract (Fatoki and Badmus, 2022; Gill, 2024). Keratin-rich tissues, such as hair, nails, and skin, act as long-term reservoirs for arsenic due to the strong binding affinity of arsenic for keratin-associated sulfhydryl groups (Madrigal-Redondo et al., 2023). This accumulation can perpetuate chronic toxicity, even after exposure ceases, contributing to long-term health effects and increased risks of organ dysfunction (Bhattacharya et al., 2020; Madrigal-Redondo et al., 2023).

2.2.2 Acute Exposure to Arsenic Trioxide

Acute exposure to arsenic trioxide disrupts cellular energy metabolism by inhibiting pyruvate and succinate oxidation, reducing acetyl-CoA and succinyl-CoA production, impairing gluconeogenesis, and disrupting oxidative phosphorylation (Madrigal-Redondo et al., 2023. Arsenic accumulates in mitochondria, damaging their membranes and mimicking phosphate anions, which leads to the loss of high-energy phosphate bonds, uncoupling ATP synthesis, and decreasing mitochondrial respiration (Madrigal-Redondo et al., 2023). Target organs include the gastrointestinal tract, heart, brain, and kidneys, with potential secondary effects on the skin, bone marrow, and peripheral nervous system. Additionally, arsenic damages endothelial cells, increasing vascular permeability (El-Ghiaty et al., 2022; Gill, 2024).

Acute arsenic poisoning presents a variety of clinical manifestations across multiple systems in the body. Gastrointestinal symptoms commonly include burning lips, pharyngeal constriction, severe abdominal pain, nausea, and a metallic or garlic-like taste. Patients may experience intense thirst, vomiting, and "rice water" diarrhea, often accompanied by mucosal inflammation, necrosis, gastrointestinal perforation, and bleeding. The fluid loss and electrolyte imbalances that result can lead to shock and, in severe cases, death (Bagga and Chawla, 2025).

Neurologically, acute exposure can cause encephalopathy, cerebral edema, headache, lethargy, delirium, hallucinations, seizures, and even coma, with hemorrhagic necrosis found in both cerebral gray and white matter (Mochizuki, 2019). Peripheral neuropathy resembling Guillain-Barré syndrome is also common, with initial sensory symptoms like tingling or electric shock-like pain in the extremities that may progress to numbness and motor weakness (Mochizuki, 2019; Thakur et al., 2021). Cardiovascular effects include increased capillary permeability and vasodilation, which may result in hypovolemic shock. Early signs can manifest as sinus

tachycardia, potentially advancing to more severe arrhythmias like polymorphous ventricular tachycardia, ventricular fibrillation, or congestive heart failure (Vineetha and Raghu, 2019). Electrocardiogram (ECG) abnormalities, such as QT interval prolongation, ST depression, and T-wave flattening, may be observed ((Vineetha and Raghu, 2019). Respiratory complications can occur due to pulmonary edema, acute respiratory distress syndrome (ARDS), and respiratory failure stemming from weakened respiratory muscles. Inhalation exposure may lead to symptoms like coughing, chest pain, and irritation of the upper respiratory tract (Mingxing et al., 2019).

Renal effects from arsenic exposure often include glomerular damage, proteinuria, and tubular necrosis, frequently leading to acute renal failure, oliguria, and hematuria. Although hepatocellular injury is rare, acute exposure may result in fatty infiltration, central necrosis, and cirrhosis, with hepatitis developing from disrupted intrahepatic metabolism and altered bilirubin transport (Elia et al., 2018; Jin et al., 2020). Musculoskeletal manifestations typically consist of myalgia, muscular weakness, atrophy, and rhabdomyolysis. Dermal symptoms can include flushing, excessive sweating, edema (particularly periorbital), hyperkeratosis, and exfoliative dermatitis. Finally, ocular effects may present as conjunctivitis, photophobia, blurred vision, diplopia, and tearing in cases of acute exposure (Reyes-Hinojosa et al., 2019; Ghiaur et al., 2024).

2.3 THE KIDNEY

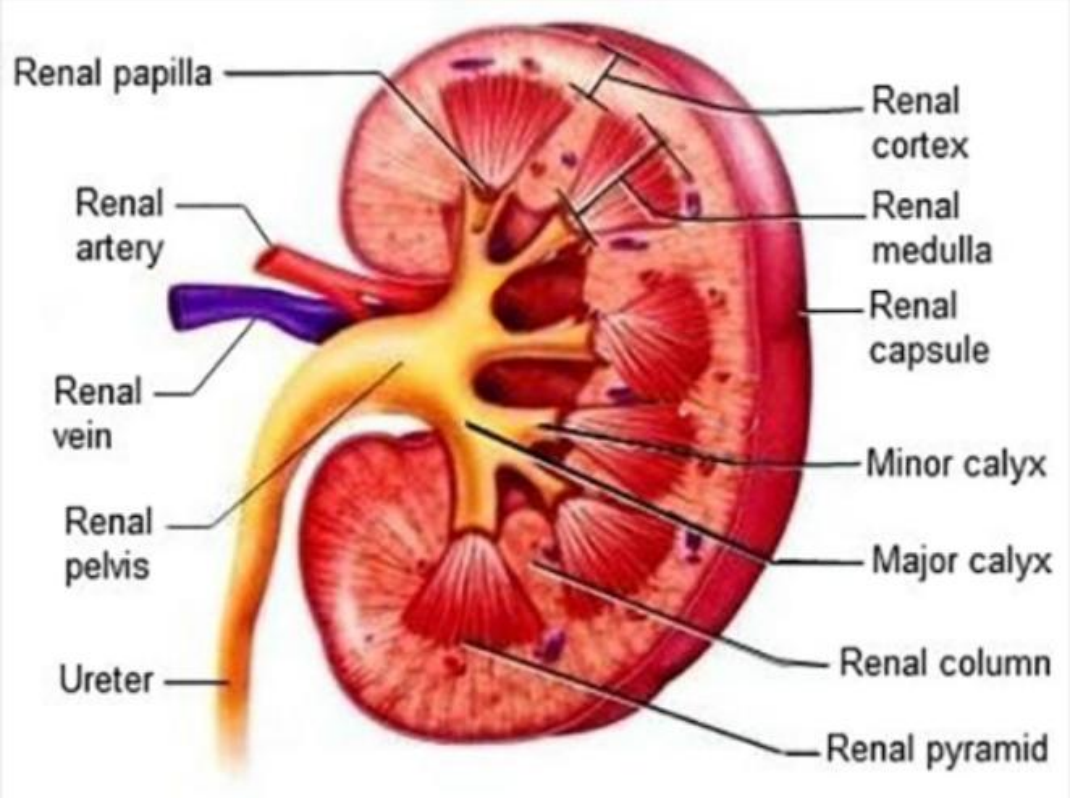

Fig 2.2: The left Kidney (News Medical, 2018)

The kidneys are bean-shaped organs characterized by a medial concavity and a lateral convexity. They weigh approximately 150–200 g in males and 120–135 g in females (Gallardo and Vio, 2022) and measure about 10–12 cm in length, 5–7 cm in width, and 3–5 cm in thickness—roughly the size of a closed fist (Monpeo et al., 2016; McBride, 2016). Positioned retroperitoneally on the posterior abdominal wall, the kidneys span the area between the transverse processes of T12 and L3 (Gallardo and Vio, 2022), with the upper poles typically oriented slightly medially and posteriorly relative to the lower poles (McBride, 2016). A lateral

orientation of the upper poles may suggest conditions such as a horseshoe kidney or a superior pole renal mass (Buffi et al., 2018; El-Zaatari et al., 2020). The right kidney is usually located slightly lower than the left due to the presence of the liver (Gallardo and Vio, 2022). Superiorly, the adrenal (suprarenal) glands cap the kidneys, with the right gland being pyramidal and apical in position and the left gland crescent-shaped and medial (Monpeo et al., 2016).

Anteriorly, the right kidney lies behind the ascending colon, with the second part of the duodenum medially and the liver separated by the hepatorenal recess (Monpeo et al., 2016; Buffi et al., 2018). In contrast, the left kidney is located posterior to the descending colon. Its hilum is lateral to the tail of the pancreas (Buffi et al., 2018), its superomedial aspect adjacent to the greater curvature of the stomach (Maurya et al., 2018), and its upper pole near the spleen, connected by splenorenal ligaments (Buffi et al., 2018). Posteriorly, the diaphragm covers the upper third of each kidney (Gallardo and Vio, 2022), with the 12th rib crossing over the upper poles (Buffi et al., 2018). The kidneys rest on the medial side of the psoas muscle and the lateral aspect of the quadratus lumborum, while the proximal ureters pass over the psoas muscle as they descend toward the pelvis (Buffi et al., 2018).

At the medial margin of each kidney is the renal hilum, where the renal artery enters, and the renal vein and pelvis exit. The renal vein is positioned anterior to the renal artery, which is in turn anterior to the renal pelvis (Gallardo and Vio, 2022). The renal pelvis, the uppermost portion of the ureter, branches into 2–3 major calyces, each of which divides into 2–3 minor calyces (Buffi et al., 2018). These minor calyces are indented by renal papillae, the tips of the renal pyramids (Maurya et al., 2018). Each pyramid and its associated cortical tissue form a lobe (Buffi et al., 2018). The kidneys are encased by a two-layered capsule and are surrounded by

layers of perinephric fat, Gerota's fascia, Zuckerkandl fascia, and paranephric fat, which together constitute the retroperitoneal space (McBride, 2016).

At the medial margin of each kidney lies the renal hilum, where the renal artery enters and the renal vein and pelvis exit (Bazira, 2022). The renal vein lies anterior to the artery, which in turn is anterior to the renal pelvis (Bazira et al., 2022; Gallardo et al., 2022). The renal pelvis, the superior portion of the ureter, branches into 2–3 major calyces, each of which divides into 2–3 minor calyces that are indented by renal papillae, the tips of the renal pyramids (Gallardo et al., 2022). Each pyramid, along with its associated cortical tissue, forms a lobe (Buffi et al., 2018; Bazira et al., 2022). The kidneys are enclosed by a two-layered capsule and surrounded by layers of perinephric fat, Gerota's fascia, Zuckerkandl fascia, and paranephric fat, all of which constitute the retroperitoneal space (Buffi et al., 2018).

2.3.1 Structure and Function

The kidney consists of two primary regions: the cortex and the medulla. The cortex houses renal corpuscles, convoluted tubules, straight tubules, collecting tubules, collecting ducts, and associated vasculature (Fernandes et al., 2019). Medullary rays, which comprise straight tubules and collecting ducts, extend into the cortex from the medulla. The medulla contains the vasa recta, a capillary network essential for the countercurrent exchange system. Pyramids, conical structures within the medulla, are formed by the collecting tubules and are oriented with their bases toward the cortex and apices toward the hilum (Surface, 2018). The apices, or papillae, project into the minor calyces and drain urine through the collecting ducts at the area cribrosa. A collecting duct, along with the group of nephrons it drains, forms a lobule (Gallardo and Vio, 2022).

The functional unit of the kidney is the nephron, with approximately 2 million nephrons per kidney in an adult. Each nephron begins with an afferent arteriole that supplies a network of capillary loops called the glomerulus (Buffi et al., 2018; Surface, 2018). The glomerulus is enclosed by Bowman's capsule, a double-layered epithelial structure that, together with the glomerulus, forms a renal corpuscle. The glomerulus drains into an efferent arteriole, which subsequently gives rise to the vasa recta, supplying the renal tubules (Surface, 2018). Beyond Bowman's capsule, the tubular system consists of the proximal convoluted tubule, proximal straight tubule (or thick descending limb of the loop of Henle), thin descending limb, thin ascending limb, distal straight tubule (or thick ascending limb), distal convoluted tubule, collecting tubule, cortical collecting duct, medullary collecting duct, papillary duct, minor calyx, major calyx, renal pelvis, and ureter (Surface, 2018; Fernandes et al., 2019). The tubules originate in the cortex, descend into the medulla, make a hairpin turn at the loop of Henle, and return to the cortex near their originating renal corpuscles (Fernandes et al., 2019).

The renal corpuscle’s glomerular filtration barrier comprises fenestrated endothelium of the glomerular capillaries, the glomerular basement membrane (GBM), and the visceral layer of Bowman's capsule, which contains podocytes. Podocyte foot processes form filtration slits covered by a slit diaphragm (Fernandes et al., 2019; Gallardo et al., 2022). The GBM consists of the lamina rara externa, lamina rara interna, and lamina densa. The parietal layer of Bowman's capsule, made of simple squamous epithelium, is separated from the visceral layer by Bowman's space. Mesangial cells, found throughout the renal corpuscle, play a structural and regulatory role (Mompeo et al., 2016; Buffi et al., 2018). The juxtaglomerular apparatus includes specialized mesangial cells, juxtaglomerular cells, and the macula densa, which is formed by the

thick ascending limb returning to its glomerulus and interacting with the afferent arteriole (Buffi et al., 2018).

The kidneys perform vital functions, including waste excretion (e.g., ammonia and urea), electrolyte regulation, and acid-base balance. They play a key role in blood pressure regulation and maintaining intravascular volume via the renin-angiotensin-aldosterone system. Additionally, the kidneys are responsible for reabsorbing amino acids, electrolytes, calcium, phosphate, water, and glucose, and for secreting hormones such as calcitriol and erythropoietin (Fernandes et al., 2019).

2.3.2 Embryology

The mammalian kidney originates from the intermediate mesoderm and undergoes development (nephrogenesis) in three successive phases: the pronephros, mesonephros, and metanephros (Johnston et al., 2019). The pronephros, located in the cervical region, begins forming at the start of the fourth week of development and consists of vestigial excretory units known as nephrotomes. These structures regress by the end of the fourth week (Costigan and Rosenblum, 2022). As the pronephros regresses, the mesonephros emerges from the intermediate mesoderm, extending from the upper thoracic to the upper lumbar segments. The mesonephros comprises excretory units that elongate, form loops, and develop capillaries to create renal corpuscles (glomeruli surrounded by Bowman's capsules). These excretory tubules drain into a collecting duct called the mesonephric or Wolffian duct. By the sixth week of development, two bilateral mesonephric organs are present (Johnson, 2016; Costigan and Rosenblum, 2022).

The metanephros, the precursor to the permanent kidney, appears in the fifth week of development and derives its excretory units from the metanephric mesoderm. The ureteric bud, an outgrowth of the Wolffian duct, interacts with the metanephric mesenchyme to initiate kidney

formation (Al-Harbi and Winyard, 2016). This interaction is mediated by key signaling molecules: tyrosine kinase inhibitors RET and MET, which interact with glial-derived neurotrophic factor (GDNF) and hepatocyte growth factor (HGF), respectively. The production of GDNF and HGF is regulated by WT1, a transcription factor expressed in the metanephric mesenchyme (Costigan and Rosenblum, 2022). Mutations in the WT1 gene, located on chromosome 11p13, can lead to Wilms tumor and other syndromes. Disruption in the interaction between the ureteric bud and the metanephric mesenchyme, often due to mutations affecting GDNF regulation, can result in renal agenesis and Potter's syndrome (Costigan and Rosenblum, 2022).

Under normal conditions, the signaling interaction promotes ureteric bud dilation to form the renal pelvis and ureter. By the sixth week, the ureteric bud splits into major calyces. Premature splitting of the ureteric bud can lead to a bifid ureter (Johnston et al., 2019). Subsequent budding from the calyces forms collecting tubules, which divide further at seven weeks. These collecting tubules are eventually absorbed by developing tubules at the periphery, forming the minor calyces. Successive generations of collecting tubules consolidate into renal pyramids (Zweyer, 2014). Simultaneously, fibroblast growth factor 2 (FGF2) and bone morphogenetic protein 7 (BMP7) stimulate the metanephric tissue cap to differentiate into S-shaped tubules and capillaries, which mature into glomeruli (Sturch et al., 2021).

The distal end of the glomerulus connects to the collecting tubules, while the proximal end develops into Bowman's capsule (Sturch et al., 2021). The renal tubules elongate and differentiate into the proximal convoluted tubule, loop of Henle, and distal convoluted tubule. Together, the renal corpuscles and tubules form the nephron, the kidney's functional excretory unit (Al-Harbi and Winyard, 2016). By the twelfth week of development, nephrons become

functional and begin producing urine. Nephron formation continues throughout fetal development, resulting in approximately one million nephrons per kidney at birth (Al-Harbi and Winyard, 2016; Sturch et al., 2021).

2.3.3 Blood Supply and Lymphatics

Approximately 20% of the total cardiac output is directed to the kidneys, which are highly vascularized organs (Buffi et al., 2018). They receive blood supply from the renal arteries, which branch off the aorta inferior to the superior mesenteric artery and enter the renal hilum at the L2 vertebral level. The right renal artery is longer than the left and passes posterior to the inferior vena cava (IVC) (Costigan and Rosenblum, 2022). Near the renal hilum, both renal arteries divide into five segmental arteries. The posterior segmental artery arises first and supplies the posterior segment of the kidney, while the remaining four segmental arteries—the superior, anterosuperior, anteroinferior, and inferior segmental arteries—originate from the anterior branch of the renal artery and supply corresponding segments of the kidney. In approximately 25% of individuals, accessory renal arteries, remnants of embryonic development, persist and typically enter the poles of the kidney, originating either from the aorta or the renal artery (Buffi et al., 2018; Al-Harbi and Winyard, 2016).

The renal veins run anterior to the renal arteries, with notable asymmetry between the left and right veins. The left renal vein is longer as it crosses the midline to reach the IVC at L2 or L3, making the left kidney a preferred choice for transplantation due to the longer vein (Al-Harbi and Winyard, 2016). The left gonadal vein usually drains into the left renal vein inferiorly, along with the left suprarenal vein and left inferior phrenic vein. In 75% of individuals, branches of the lumbar or hemiazygos veins also join the left renal vein (Johnston et al., 2019). The left renal vein traverses posterior to the superior mesenteric artery and anterior to the aorta, a position that

makes it vulnerable to compression between these arteries, potentially leading to renal vein entrapment syndrome. In contrast, the right gonadal and renal veins typically drain separately into the IVC (Buffi et al., 2018).

Lymphatic drainage of the kidneys, often accompanied by lymphatics from the proximal ureters, terminates in the aortic lymph nodes on the left and the right lateral inferior caval lymph nodes on the right. This intricate vascular and lymphatic network underscores the kidneys' critical role in systemic circulation and waste filtration (Buffi et al., 2018; Costigan and Rosenblum, 2022).

2.3.4 Nerves

The innervation of the kidneys, proximal ureters, and suprarenal glands is mediated by the renal nerve plexus, which contains both sympathetic and parasympathetic fibers. These fibers come from the abdominopelvic splanchnic nerves (Costigan and Rosenblum, 2022). The sympathetic nerves specifically innervate the renal vasculature, with a focus on areas such as the afferent arterioles, the thick ascending limbs, and the distal convoluted tubules of the nephron. Sensory afferent nerves are primarily located in the renal pelvis and travel along the renal artery or proximal ureter toward the pelvic wall, playing a crucial role in sympathetic regulation and blood pressure control (Buffi et al., 2018). These sensory fibers can be aligned in parallel or circumferential orientations, and they innervate the pelvic wall, renal artery, and renal vein. Notably, there are no sensory fibers in the medulla, and very few are found in the cortex (Gallardo and Vio, 2022).

Pain sensation in the kidneys is mediated by visceral afferent fibers, which transmit pain along the sympathetic fibers to the spinal ganglia, typically in segments T11-L2 (Johnston et al., 2019). This can cause referred pain, where kidney-related discomfort manifests as flank pain in the corresponding dermatome. Renal pain is often a result of obstruction, dilation, inflammation,

infection, or ischemia. However, non-obstructing kidney stones usually do not cause significant renal pain or colic (Gallardo and Vio, 2022).

CHAPTER THREE

MATERIALS AND METHOD

3.1 EQUIPMENTS

The Following Materials Were Used for Study:

Animals: 30 adult wistar rats; Feed: pelleted food, instruments: Plastic cages, ceramic plates, Waltman filter paper, funnel, conical flask, surgical blade, forceps, 5ml syringe, laptop, weighing balance, microtome, slide tray, tissue embedding station, microscope, specimen bottles, cotton wool, orogastric tube, disposable gloves, measuring cylinder, Reagents: 10% formal saline, chloroform, distilled water, eosin, hematoxylin, paraffin wax, xylene, nose mask.

3.2 MANUFACTURER'S INFORMATION

Silymarin (manufactured by micro labs LTD Mamring, Namthang Road, South Sikkim-737 132 India).

Arsenic Trioxide (manufactured by Loba Chemie PVT LTD India).

3.3 METHOD

3.3.1 EXPERIMENTAL ANIMALS

Thirty-adult Wistar rats were used as experimental animals in this study. Their weight ranged between 130g and 150g.The rats were purchased and maintained at the Animal House in the Department of Anatomy, School of Basic Medical Sciences, College of Medical Sciences, University of Benin, Edo State. The rats were then put in their cages. Before transferring the rats into their cages, cages were cleaned and disinfected. They were fed with pelleted food (manufactured by Premier Feed Mills Company Limited, 1 Eagle Flour Road, Lagos Ibadan expressway, tell point, Ibadan, Oyo state, Nigeria) throughout the acclimatization period which

lasted for 7 days as much as they were allowed access to clean tap water. The cages were made of plastic and wire gauze at the top to allow proper ventilation and the cages were cleaned daily and disinfected at intervals. Each animal procedure was carried out in accord with approved protocols and in compliance with the recommendation for the proper management and utilization of laboratory animals used for research.

The animals were weighed before commencement of the experiment. Protocols for this experiment were in accordance with the guide for the care and use of laboratory animals (National Research Council of the National Academics, 2011).

3.3.2 METHOD OF EXTRACTION

Persea americana seeds were gotten from mature fruits obtained from Uselu market, Egor Local government area, Benin city, Edo State.

They were subsequently identified and authenticated at the herbarium, Department of Plant Biology and Biotechnology, University of Benin, and given Herbarium number: **UBH-P408.** After identification, the seed was removed from the fruit and was thoroughly washed with tap water, it was air dried and then pulverized to powered form. The powered formed obtained was weighed and soaked in distilled water for 24hrs. The solution was then filtered. The residue was discarded then the filtrate was freeze dried with freeze drying machine and refrigerated.

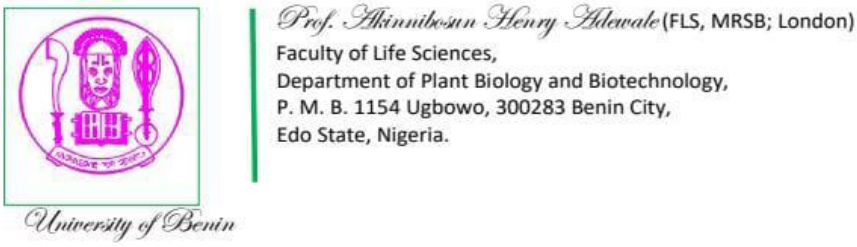

Prof. Akinnibosun Henry Adewale (FLS, MRSB; London)
Faculty of Life Sciences,
Department of Plant Biology and Biotechnology,
P. M. B. 1154 Ugbowo, 300283 Benin City,
Edo State, Nigeria.

University of Benin

Department of Plant Biology and Biotechnology

Herbarium Unit

Faculty of Life Sciences

University of Benin, Benin City, Edo State

Plant Name: *Persea americana* Mill.

Family: Lauraceae

Common Name: Avocado pear, Alligator pear

Voucher Number: UBH-P408

Student Name:

Plant Identification By: Prof. Emmanuel Isaka Aigbokhan

Voucher Number Issued by:

18/12/2024

Prof. Henry Adewale AKINNIBOSUN (FLS, MRSB; London, LMBOSON, MECOSON, MAEIAN, MFBAN; Nigeria)

Fig 3.1: Image of Plant Identification Number.

3.3.3 EXPERIMENTAL DESIGN

The thirty rats were randomly divided into six groups; A, B, C, D, E, and F with each group containing a total of five rats. The administration was done orally and lasted for 28 days and after completion of the administration the kidney was harvested from each groups for histological assessment.

TABLE 3.1 EXPERIMENTAL DESIGN

GROUPS	TREATMENTS
Group A	Control.
Group B	Received 10mg/kg of arsenic trioxide.
Group C	Received 140mg/kg body weight of Silymarin + 10mg/kg of arsenic trioxide.
Group D	Received 125mg/kg body weight of *Persea americana* + 10mg/kg of arsenic trioxide.
Group E	Received 250mg/kg body weight of *Persea americana* + 10mg/kg of arsenic trioxide.
Group F	Received 10mg/kg of arsenic trioxide for 7 days and allowed to recover.

3.3.4 SACRIFICE AND SAMPLE COLLECTION

At the end of the twenty-eight (28) days of treatment, the rats were weighed and the weight recorded. Later on, the rats were euthanized under chloroform anesthesia. An abdominal incision was made and the kidneys was properly harvested and weighed. Following the weighing procedure, the kidneys samples were fixed immediately to prepare them for histological assessments.

3.3.5 TISSUES PROCESSING.

The tissues were processed using the paraffin wax embedding method of Drury and Wallington (1980). The harvested tissues were preserved in 10% phosphate-buffered formalin for histopathology. The tissues were dehydrated for one hour at room temperature using ascending grades of ethanol: 70% ethanol, 90% ethanol, Absolute ethanol I, and Absolute ethanol II. The dehydrated tissues were cleared at room temperature in two changes of xylene for one hour in each change. Finally, the tissues were embedded in paraffin wax multi-block plastic embedding molds. In order to section the tissues on a rotating microtome, the paraffin-blocked tissues were cut and put on a wooden chaunk. From the tissue blocks, sections with a thickness of 5 µm were cut using a rotary microtome (Bright B5143, Huntington, England). In order to facilitate the spreading of the folded ribbon of portions, the sections were placed into a water bath at 40 degrees Celsius. These segments were installed on brand-new, spotless glass slides. To improve the adherence of the sections to the slides, these were dried at 40oC using a slide drier.

3.4 HAEMATOXYLIN AND EOSIN STAINING PROCEDURE.

Tissue sections were deparaffinized in two changes of xylene for two minutes in each change and passed through two changes of absolute alcohol for four minutes each. They were hydrated using a series of descending grades of alcohol until the water was used. Procedures of Haematoxylin and Eosin adopted in the sections were described by Drury and Wallington (1980) and Scheehan and Hrapchak (1980). The sections were:

• Dewaxed in two changes of xylene for two minutes in each change;

• Rehydrated in descending grades of alcohol (absolute II, absolute I, 95%, 90%, 70%, and 50% ethanol) for two minutes each;

• Rinsed in distilled water for three minutes

• Stained in hematoxylin for 15-20 minutes

• Excess hematoxylin stain was removed by rinsing well in running tap water for two to three minutes (sections were examined microscopically at this stage to confirm a sufficient degree of staining);

• Differentiated in acid alcohol (0.5% HCl in 70% ethanol for two to three minutes;

• Rinsed well in running water for 10-15 minutes;

• Counterstained in 1% aqueous eosin for two to four minutes;

• Excess stain was washed off in running water and examined under a microscope;

• Dehydrated rapidly in ascending grades of ethanol (50% through absolute ethanol), cleared in xylene, and mounted in a synthetic resin medium (DPX).

3.5 PHOTOMICROGRAPHY

Histological sections were examined under Leica DM750 research microscope with a digital camera (Leica ICC50) attached. Photomicrographs of the tissue sections were taken at various magnifications i.e 100X and 400X.

3.6 STATISTICAL ANALYSIS

3.6.1 OXIDATIVE STRESS

DETERMINATION OF CATALASE (CAT)

Catalase (CAT) activity was estimated by the method described by Cohen et al., (1970).

Reagents

Hydrogen peroxidase (H_2O_2)

Suphuric acid (6M) H_2SO_4

Preparation of reagents

0.01M $KMnO_4$ was prepared by distilling 0.158g of $KMnO_4$ in 100ml of distilled water. Phosphate buffer (pH 7.4) 0.426g of $NaHPO_4$ and 0.240g of NaH_2PO_4 was weighed and dissolved in 100ml of distilled water. 6M H_2SO_4 and 32.3ml of conc. H_2SO_4 were added to 66.7ml of distilled water.

Procedure

To an unknown volume of plasma (0.5ml), 5.0ml of H_2O_2 was added. This was mixed by inversion and allowed to stand for 30min. The reaction was stopped by adding 1.5ml of 6M H_2SO_4 and 7ml of 0.01M $KMnO_4$. These were mixed by inversion and allowed to stand for 10min. The absorbance was read at 480nm within 30-60 seconds against distilled water. The enzyme blank was run simultaneously with 1.0ml of distilled water instead of hydrogen peroxide. The enzyme activity was expressed as μmoles of H_2O_2 decomposed/min/mg/protein.

Calculation

$$\text{Activity} = \frac{\text{OD/min x V}}{\text{M x V x L x Y}}$$

Where OD = Absorbance

L= Light path

V= Total volume of reaction sample

M= Molar coefficient of H2O2 (40/m/cm)

V= Volume of sample

Y= mg protein in the sample

ESTIMATION OF SUPEROXIDE DISMUTASE ACTVITY (SOD)

This was determined according to teh methods of Masra and Fridorich (1972)

Principle

Adrenaline undergoes auto oxidation rapidly to adrenochrome whose concentration can be determined at 420nm with the aid of a spectrophotometer. The auto oxidation of adrenaline depends on the presence of super anions.

Superoxide dismutase inhibits the auto-oxidation of adrenaline by catalyzing the breakdown of superoxide anion. The degree of inhibition reflects the activity of SOD which is determined at 420nm.

Reagent and preparation

Carbonate buffer (0.05M) pH 10.2: This was prepared by dissolving 0.2014g of Na2CO3, 0.2604g NaHCO3 and 0.0372g of EDTA in 100ml of distilled water. The pH was adjusted to 10.2 using Sodium hydroxide.

Hydrochloric acid (0.005M): This was prepared by adding 0.044 concentration of HCL to 99.96mls of distilled water.

Adrenaline solution (0.3mM): This was prepared by dissolving 0.01098g of adrenaline in 100mls of 0.005M HCL solution.

Plasma volume of 100ml was mixed with 125ml of carbonate buffer and 150ml of adrenaline solution. 100ml of distilled water was mixed with 1.25ml of carbonate buffer as reference sample. These were mixed and absorbance read at 420nm.

These were mixed and read at 420nm

$$\%\text{inhibition} = \frac{(\text{O.D test} - \text{ODref}) \times 100}{\text{OD test}}$$

Enzyme concentration can thus be calculated

$$\text{unit/mg protein} = \frac{\%\ \text{inhibition}}{50 \times Y}$$

Where Y = mg of protein in the volume of sample used.

ESTIMATION OF GLUTHATHIONE PEROXIDASE (GPx)

This was determined according to Nyman (1959)

Principle

This is based on the oxidation of pyrogallol to purpurogallin by peroxidase activity, resulting to a deep brown color disposition, read at 420nm.

Reagent and preparation

Pyrogallol (20mM): 0.2552g of pyrogallol was dissolved in 100mls of distilled water.

Procedures

To an aliquot of plasma (0.2ml), 2.5ml of phosphate buffer, 2.5ml of H_2O_2, 1.5ml of distilled water and 2.5ml of pyrogallol was added.

The reaction was allowed to stand for 30mins at room temperature. A deep brown color was formed which was read at 480nm.

Calculations

$$\text{Activity} = \frac{OD/min \times vt \times Df}{E \times Vs \times Y}$$

OD= Absorbance of test

Vt= Total volume of reaction mixture

Df= Diution factor = 1

E= Molar extinction co-efficient (12/m/cm)

Vs= Volume of sample

Y= mg of protein used

DETERMINATION OF MALONDIALDEHYDE (MDA)

Malonaldehyde was determined using the thiobarbituric acid assay (Buege and Aust, 1978)

Principle

Malonaldehyde which is a product of lipid peroxidation react with thiobabituric acid (TBA) to give a red species.

Procedure

A volume of plasma (1.0ml) was added to 2.0ml of TCA-TBA-HCL and mixed thoroughly. The solution was heated for 15mins in a boiling water bath. After cooling, the flocculent precipitate was removed by centrifuged at 1000g for 10min. The absorbance was determined using the formula;

$$\text{MDA (mol/mg protein)} = \frac{A \times V \times 100}{M \times V \times Y}$$

A= Absorbance

V= Total volume of reaction mixture

M= Molar extinction coefficient

V= volume of the sample

Y= mg protein

3.6.2 KIDNEYFUNCTION TEST

Urea Estimation (Lamb and Price, 2008).

Urea was measured using Selectra ProS auto-analyzer, manufactured by EliTech Clinical System, SAS, France, following manufacturer instructions.

Method: Urease Enzymatic method (kinetic).

Assay Principle: Urea is hydrolyzed by Urease to produce ammonium, the ammonium generated react with α-ketoglutarate in the presence of reduced nicotinamide adenine dinucleotide, catalyzed by glutamate dehydrogenase. The nicotinamide adenine dinucleotide generated is monitored at 340nm. The amount of nicotinamide adenine dinucleotide released is directly proportional to the amount of urea present in the sample.

$$\text{Urea} + 2H_2O \xrightarrow{\text{Urease}} 2NH_4^+ + CO_3^{2-}$$

$$NH_4^+ + \alpha\text{-ketoglutarate} + NADH \xrightarrow{\text{GIDH}} \text{L-Glutamate} + NAD^+ + H_2O$$

GIDH = Glutamate dehydrogenase (Lamb and Price, 2008).

Creatinine Estimation (Newman and Price, 2001).

Creatinine was measured using Selectra ProS auto-analyzer, manufactured by EliTech Clinical System, SAS, France, following manufacturer instructions.

Method: Colorimetric, Jaffe-kinetic

Assay principle: Creatinine in alkaline medium react with picric acid to form picrate. The rate of formation of colour complex is measured at 505nm. The colour complex formation is proportional to the concentration of creatinine in the sample. The effects of interfering substances are reduced using the kinetic procedure (Newman and Price, 2001).

Estimation of Na+, K+, Cl- and HCO3- (Vital Scientific, 2003).

These electrolytes were measured using ion selective electrodes manufactured by SFRI Medical Diagnostics, France, model ISE 4000.

Assay principle: This is based on the principle of potentiometer which operates on the measurement of potential difference between two electrodes and the principle of partial pressure for the estimation of bicarbonate. The Na+, K+, and Cl- in the sample interact with their corresponding electrode to create a potential difference across the electrodes. The difference in the potential is proportional to the concentration of the analytes in the sample. HCO3- is measured as total CO2. The CO2 released create a tension in the bicarbonate chamber, the tension or pressure created is detected by CO2 sensor and quantified it as total CO2 which is directly proportional to the concentration of HCO3- in the sample.

Assay procedure: 150µl of sample is aspirated by the automation, analyzed and result is displayed after a minute (Vital Scientific, 2003).

CHAPTER FOUR

RESULTS

4.1 STATISTICAL ANALYSIS OF EXPERIMENTAL ANIMALS

Chart1 shows the statistical analysis of the total initial and final body weights of all experimental groups. There was no significant difference ($P<0.05$) between initial and final body weight across all experimental groups. Chart 2 shows the statistical analysis of the body weight changes of all the experimental groups. From the chart, there was a significant decrease in the arsenic-only group compared to the control ($P<0.05$) and a significant increase in the treatment group compared to arsenic-only ($P<0.05$). Chart 3 shows the statistical analysis for the kidney weight after administration. From the chart, there was no significance difference across all experimental groups ($P<0.05$). Chart 4 shows no significant difference in the Reno-somatic index after administration across all experimental groups. Chart 5 shows significant increase in urea level in the arsenic-only group and the group that was left to recover compared to control ($P<0.05$) and significant decrease in the treatment group compared to arsenic-only ($P<0.05$). Chart 6 shows significant increase in the arsenic-only group in creatinine level and the group that was left to recover ($P<0.05$ vs. control) and significant decrease in the treatment groups ($P<0.05$ vs. arsenic-only). Chart 8 & 9 the potassium and bicarbonate ion, there was a significant increase in the arsenic-only group and the group that was left to recover compared to the control group ($P<0.05$) and a significant decrease in the treatment group compared to the arsenic only group. In the case of the oxidative stress parameters (chart 11, 12, and 13), arsenic caused a significant decrease in SOD, and GPX activities and a significant increase in MDA activities when compared with control while treatment group was able to reverse these significant changes except for the recovery group.

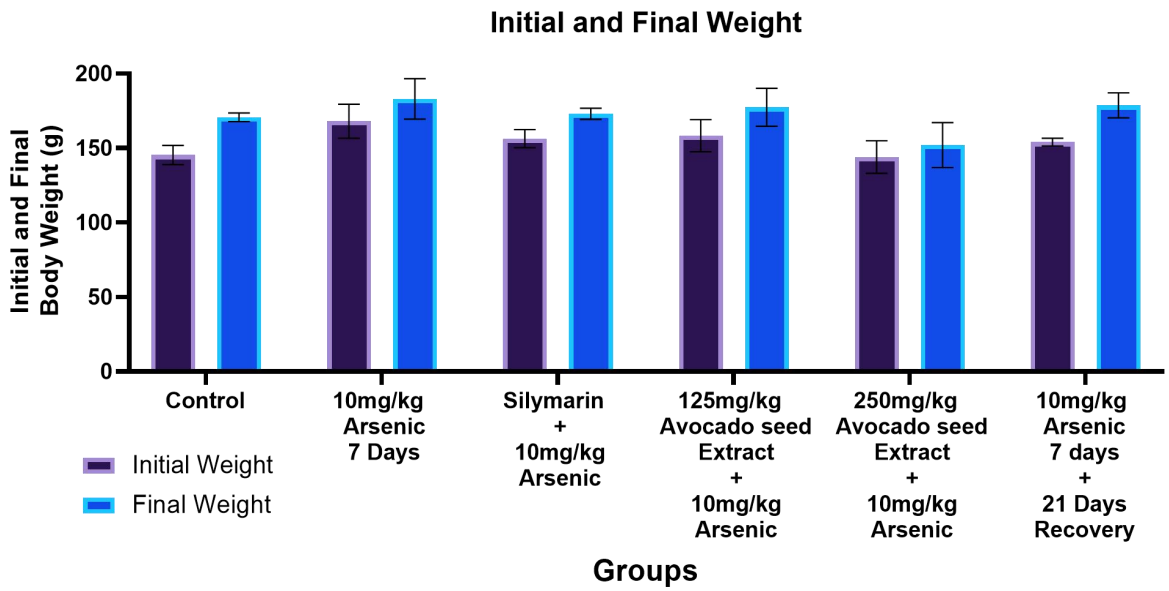

Chart 1: Initial and Final weight after administration Values are expressed as mean ± SEM.

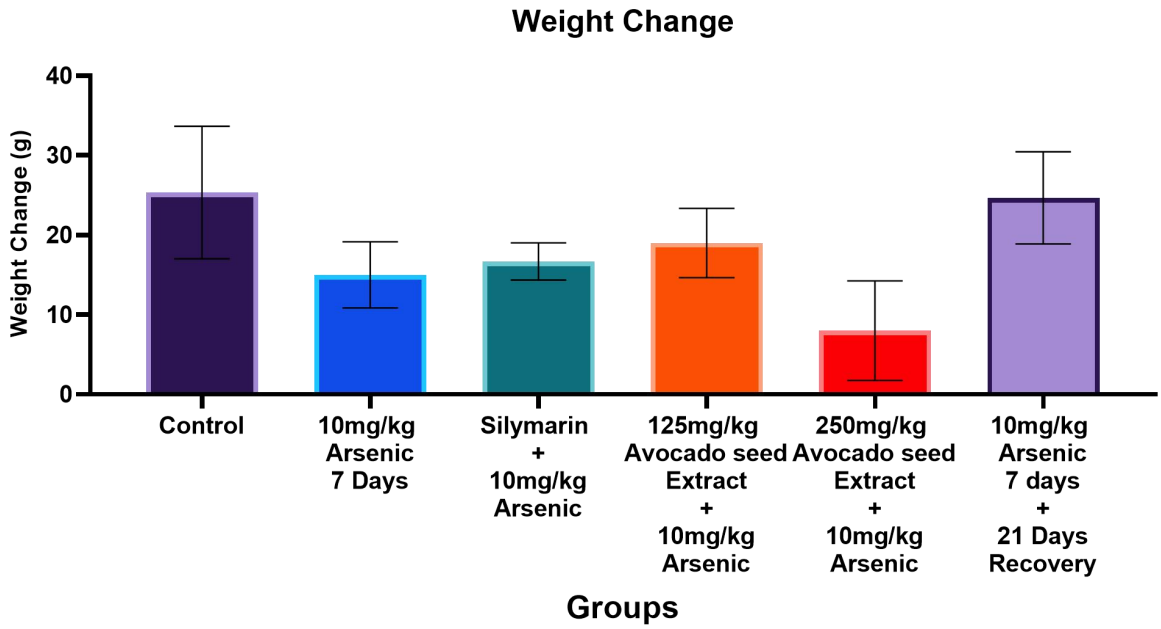

Chart 2: weight change after administration Values are expressed as mean ± SEM. *P<0.05 compared with Control; #P<0.05 Compared with 100mg/kg Arsenic Only

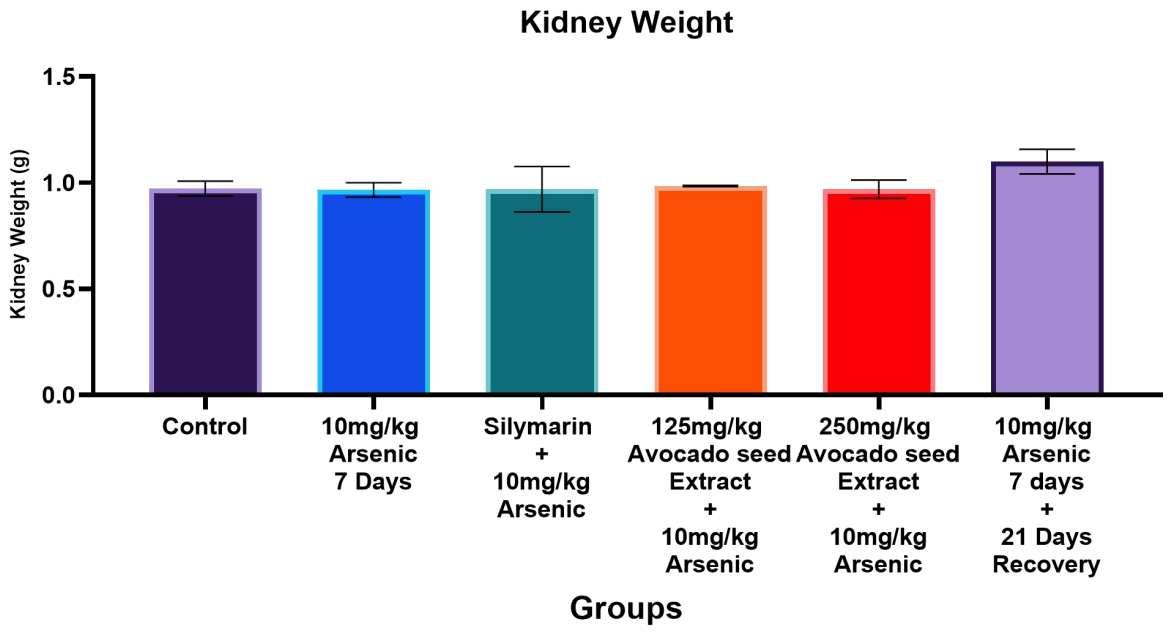

Chart 3: Kidney weight after administration Values are expressed as mean ± SEM.

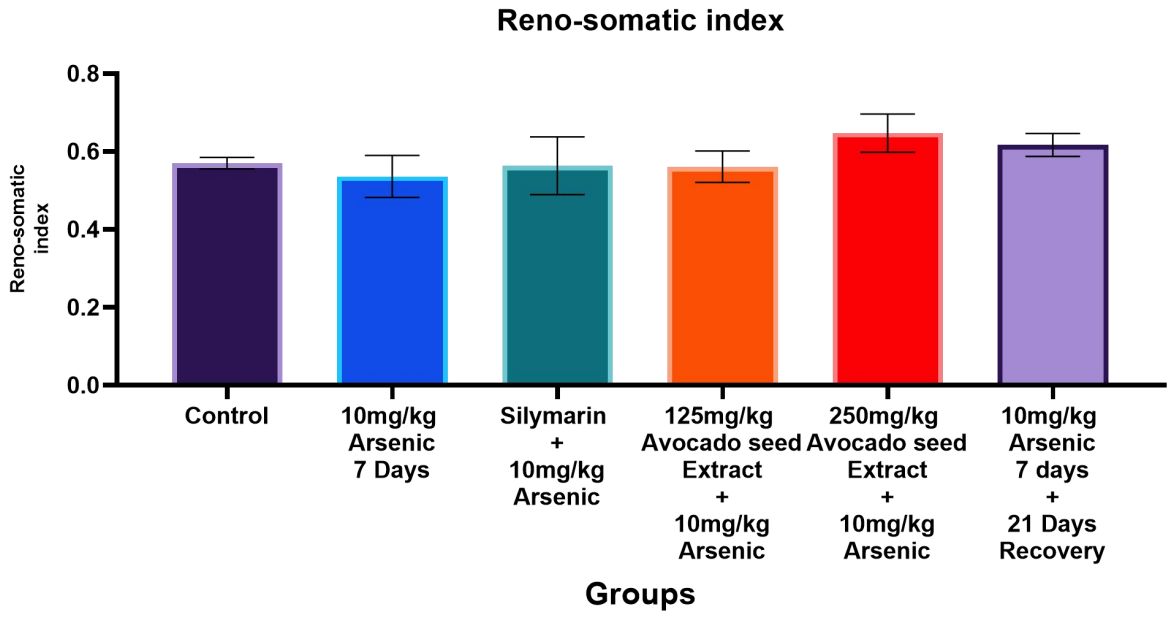

Chart 4: Reno-Somatic Index after administration Values are expressed as mean ± SEM.

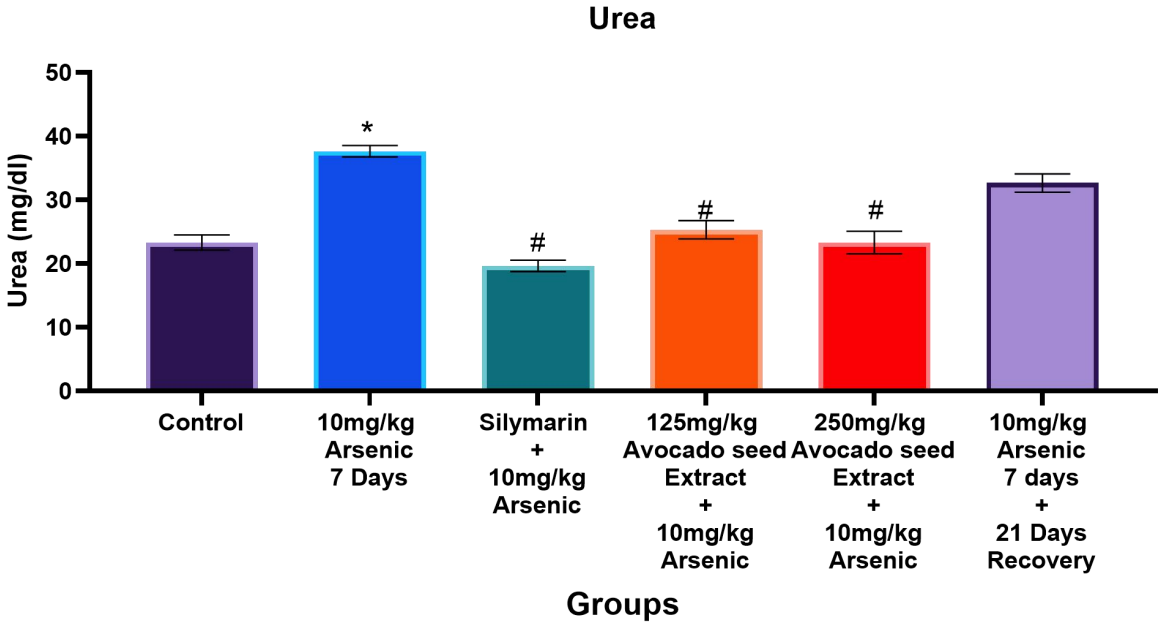

Chart 5: Urea levels in the Kidney of control and treatment groups after administration. Values are expressed as mean ± SEM. *P<0.05 compared with Control. #P<0.05 compared with Arsenic Trioxide only group.

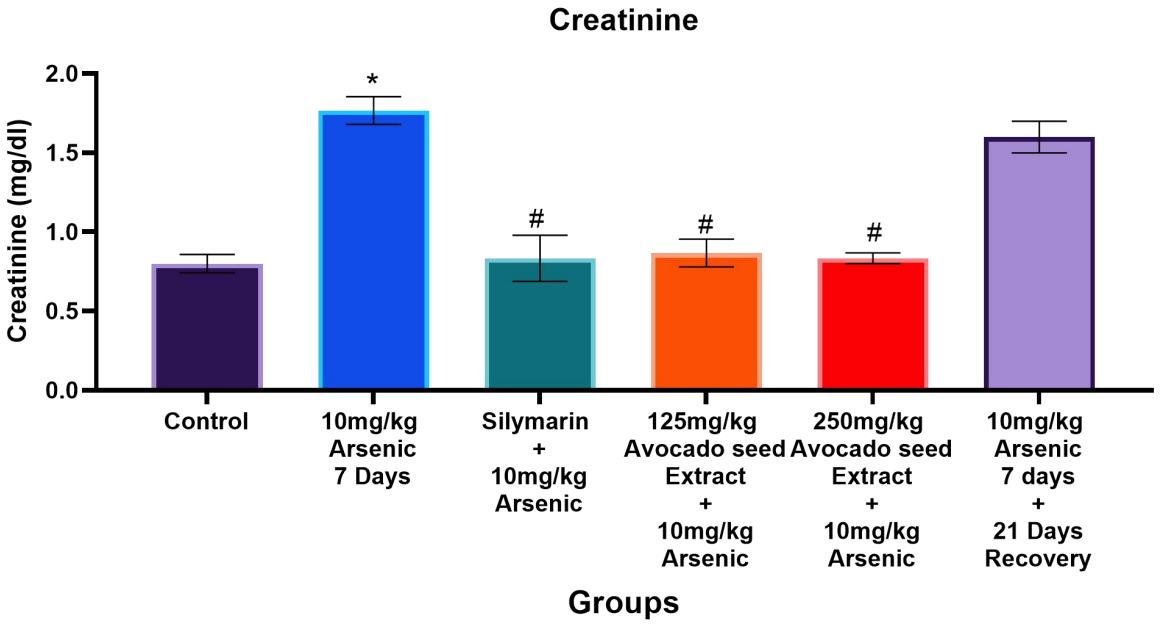

Chart 6: Creatinine level in the Kidney of control and treatment groups after administration. Values are expressed as mean ± SEM. *P<0.05 compared with Control. #P<0.05 compared with Arsenic Trioxide only group.

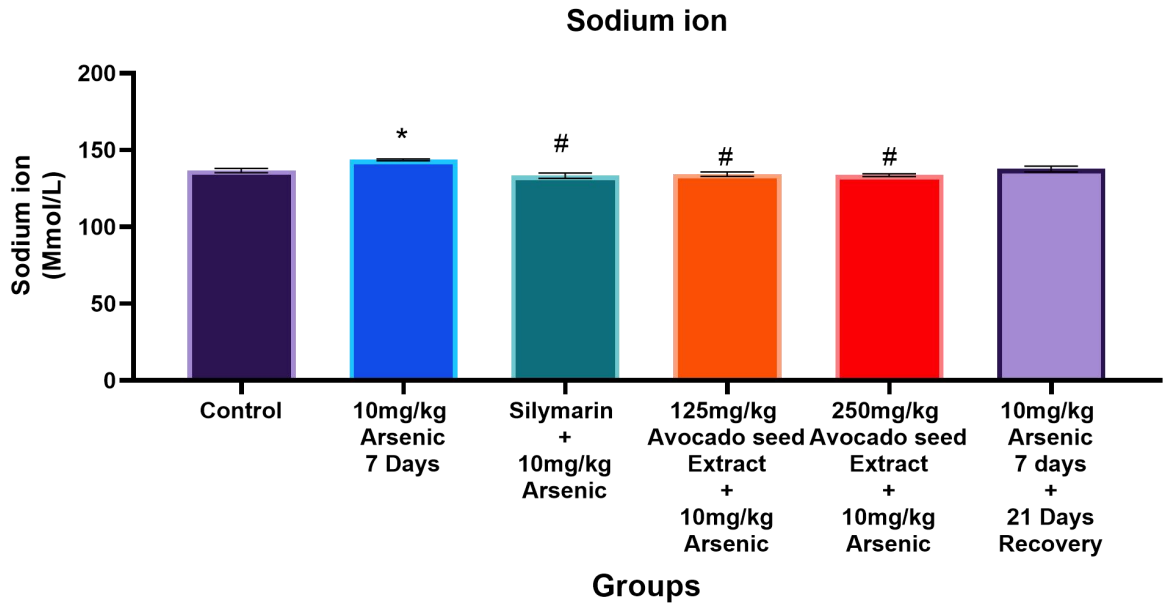

Chart 7: Sodium ion level in the Kidney of control and treatment groups after administration. Values are expressed as mean ± SEM. *P<0.05 compared with Control. #P<0.05 compared with Arsenic Trioxide only group.

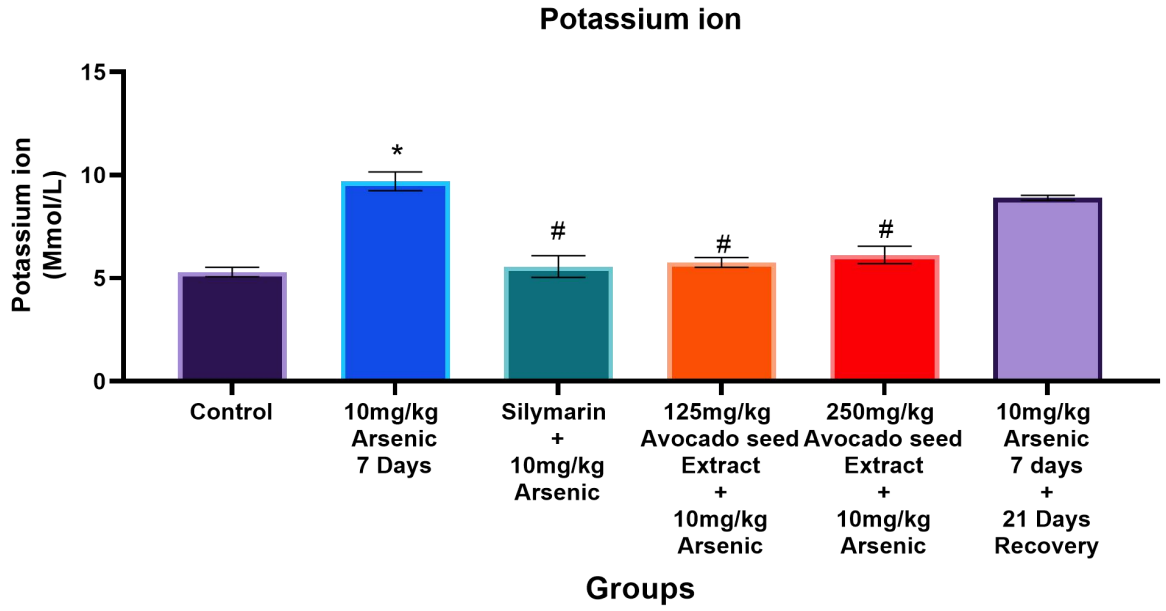

Chart 8: Potassium ion level in the Kidney of control and treatment groups after administration. Values are expressed as mean ± SEM. *P<0.05 compared with Control. #P<0.05 compared with Arsenic Trioxide only group.

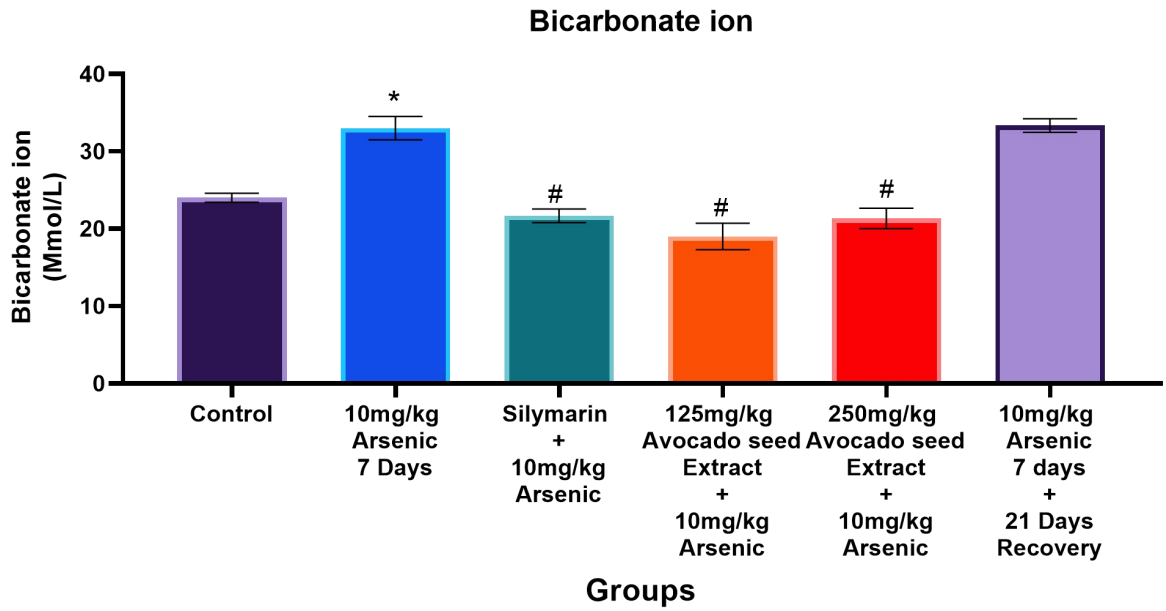

Chart 9: Bicarbonate ion level in the Kidney of control and treatment groups after administration. Values are expressed as mean ± SEM. *P<0.05 compared with Control.

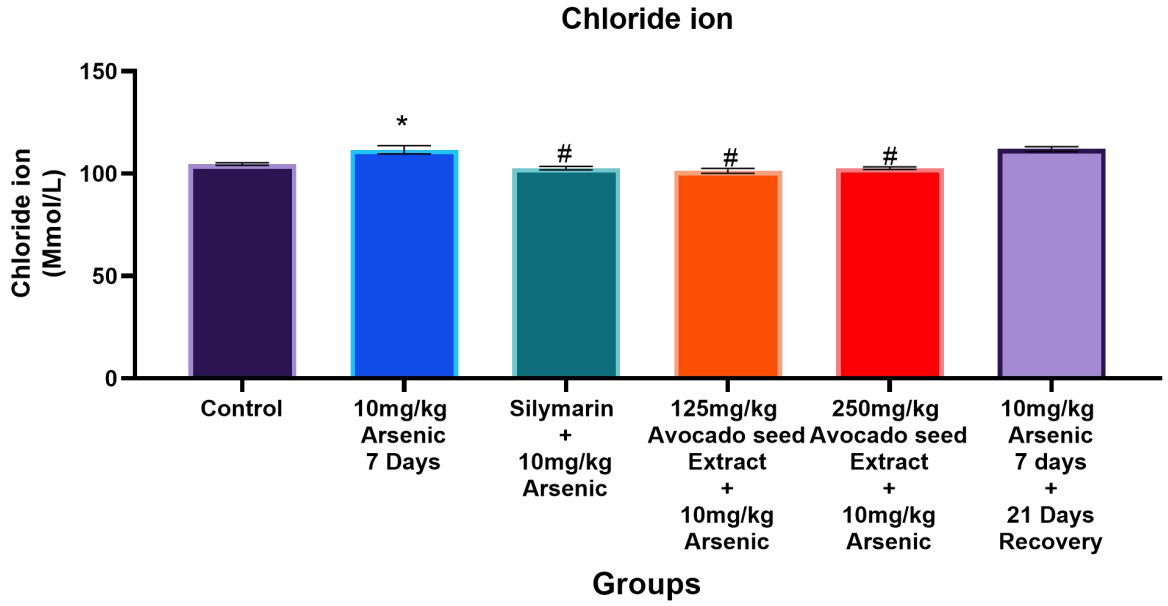

Chart 10: Chloride ion level in the Kidney of control and treatment groups after administration. Values are expressed as mean ± SEM. *P<0.05 compared with Control. #P<0.05 compared with Arsenic Trioxide only group.

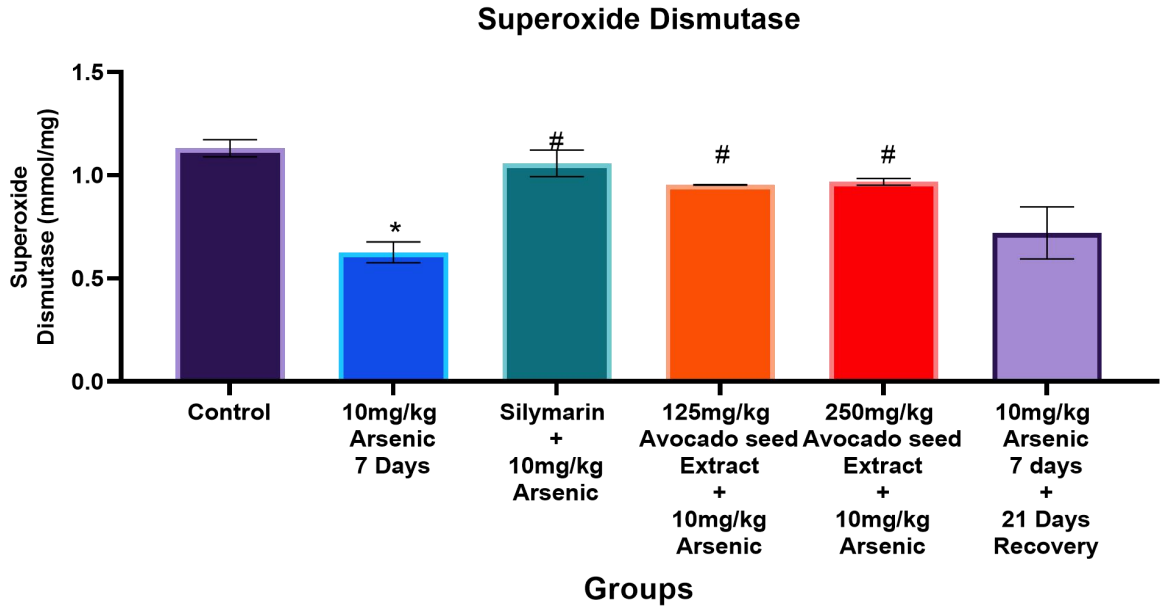

Chart 11: Superoxide dismutase activity in the Kidney of control and treatment groups after administration. Values are expressed as mean ± SEM. *P<0.05 compared with Control. #P<0.05 compared with Arsenic Trioxide only group.

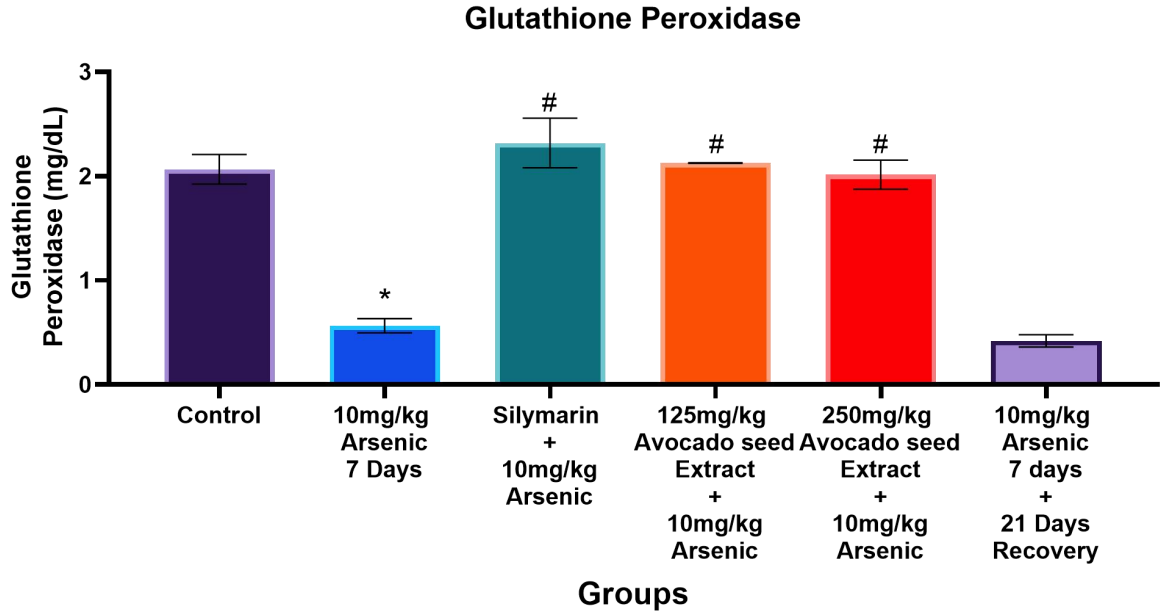

Chart 12: Glutathione Peroxidase activity in the Kidney of control and treatment groups after administration. Values are expressed as mean ± SEM. *P<0.05 compared with Control. #P<0.05 compared with Arsenic Trioxide only group.

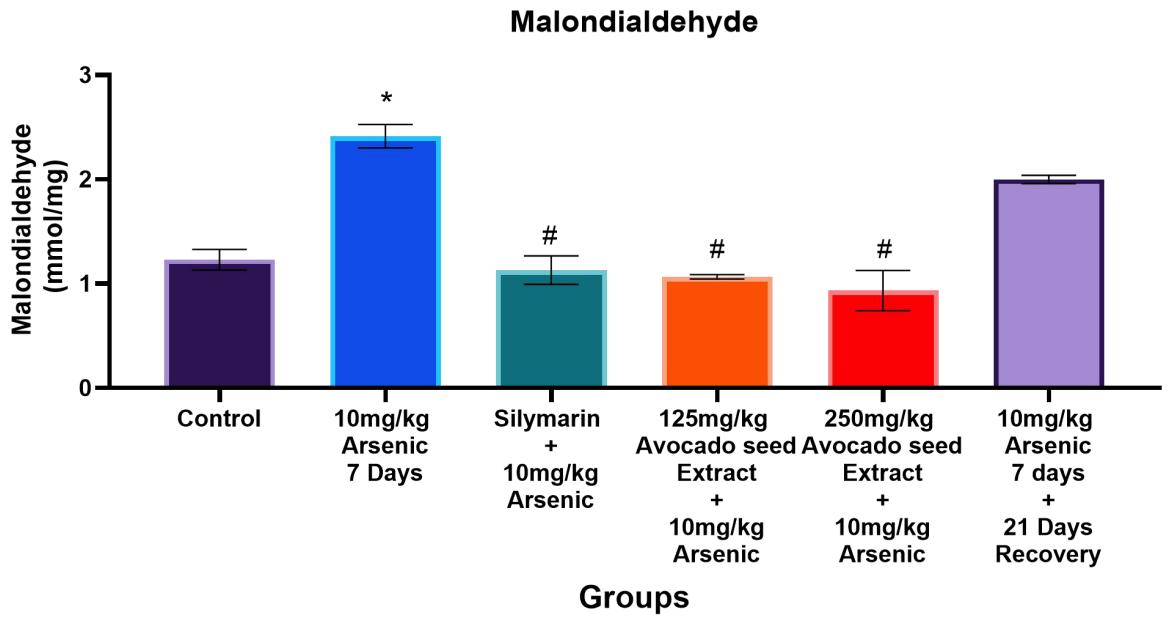

Chart 13: Glutathione Peroxidase activity in the Kidney of control and treatment groups after administration. Values are expressed as mean ± SEM. *P<0.05 compared with Control. #P<0.05 compared with Arsenic Trioxide only group.

4.2 HISTOLOGICAL FINDINGS

Sections of the kidneys taken from rats in the normal control group show normal tissue architecture with well-defined tubules, glomeruli, arcuate blood vessels and interstitial space.

Sections from rats treated with Arsenic only show interstitial infiltrates of inflammatory cells, congestion and vasodilatation, all features of inflammation of the kidney also called pyelonephritis.

Sections taken from rats treated with Arsenic, followed with graded doses of Avocado seed extract, and standard drug show normal kidney architecture with well-defined tubules, glomeruli, acuate blood vessels and interstitial space, there is an added beneficial vasoactive effect of increase in blood circulation in the kidneys (active congestion).

However, sections of the kidney tissue taken from rats treated with Arsenic only and left to recover show lingering inflammation of the kidneys as well as localized areas of tubular necrosis. Thus graded doses of Avocado seed extract and standard drug ameliorated the pyelonephritis induced by Arsenic trioxide.

4.3 RESULT OF PHOTOMICROGRAPH

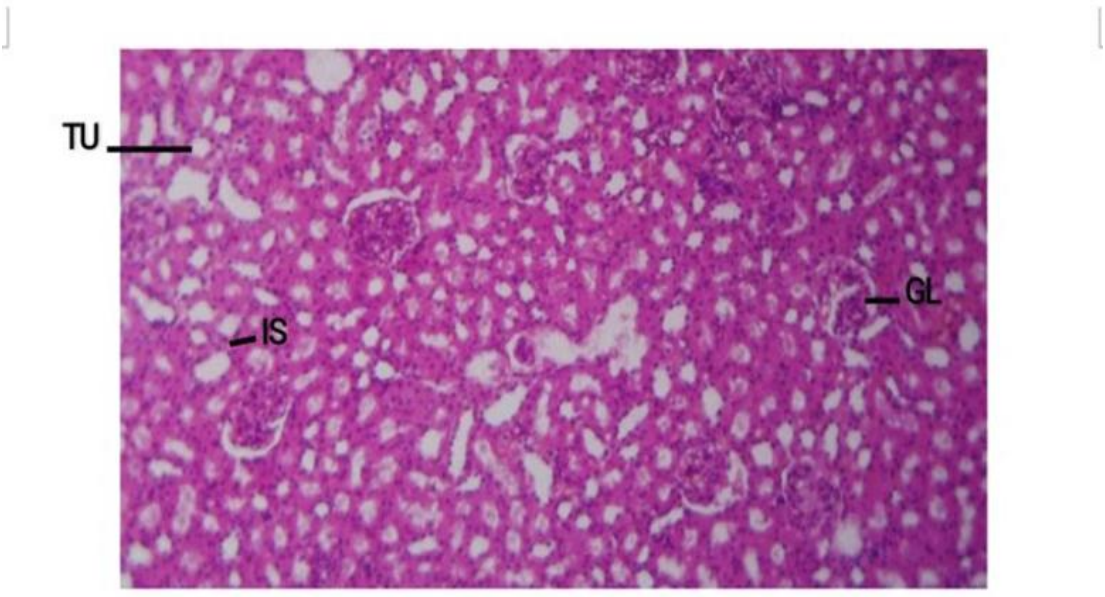

Plate 1. Rat kidneys, control show: normal architecture: tubules (TU), interstitial space (IS) and glomeruli (GL): H&E 100

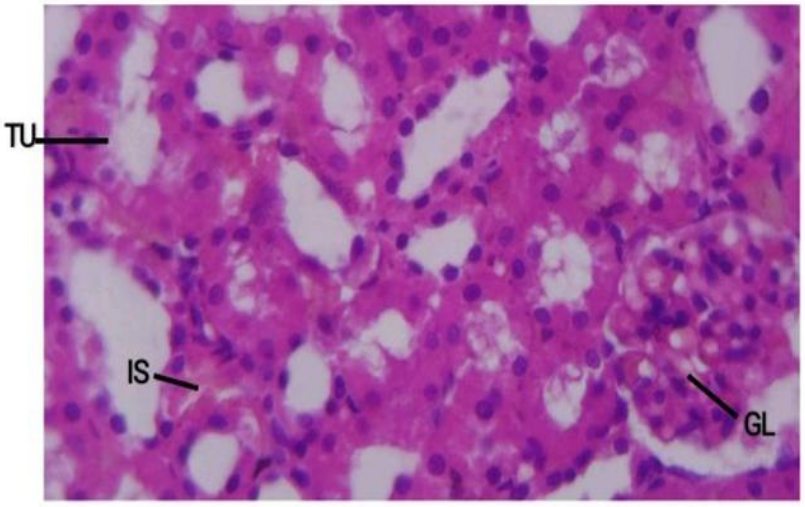

Plate 2. Rat kidneys, control show: normal architecture: tubules (TU), interstitial space (IS) and glomeruli (GL) : H&E 400

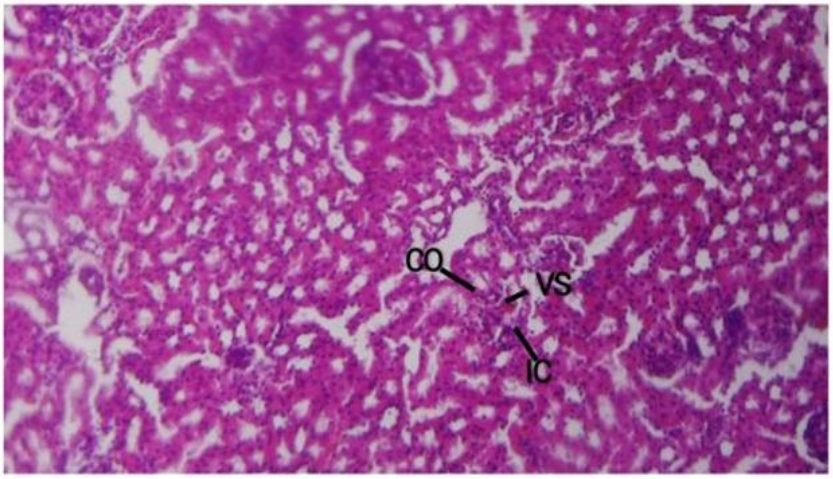

Plate 3. Rat kidney given Arsenic only show: interstitial congestion (CO), vascular stenosis (VS) and interstitial infiltrates of inflammatory cells (IC): H&E 100 X

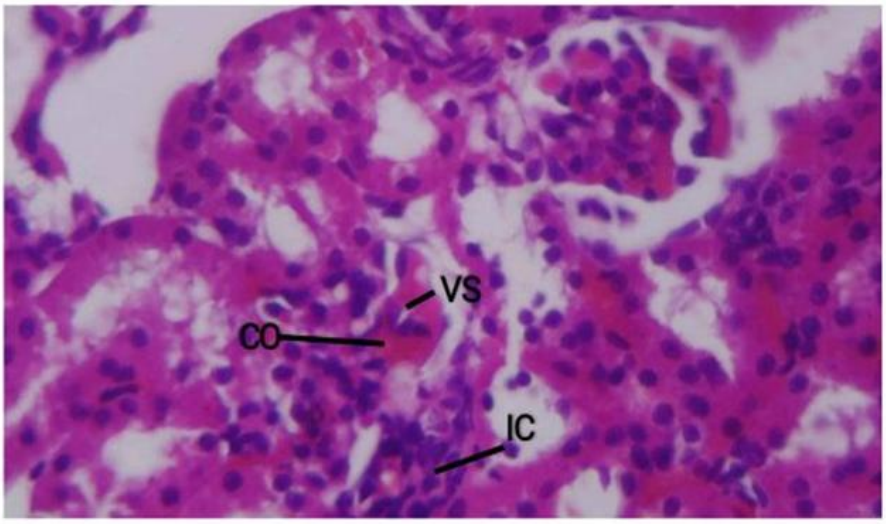

Plate 4. Rat kidney given Arsenic only show: interstitial congestion (CO) vascular stenosis (VS) and interstitial infiltrates of inflammatory cells (IC): H&E 400 X

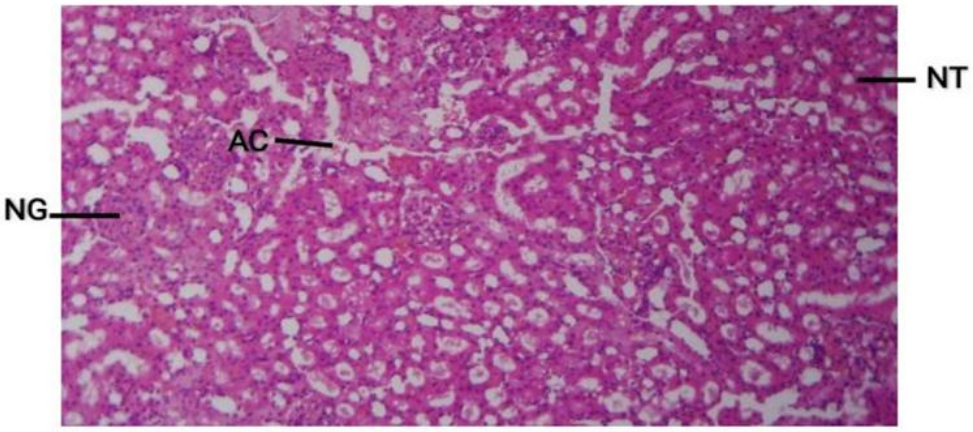

Plate 5. Rat kidneys given Arsenic + Standard drug show: active interstitial congestion (AC), normal tubules (NT) and glomeruli (NG): H&E 100 X

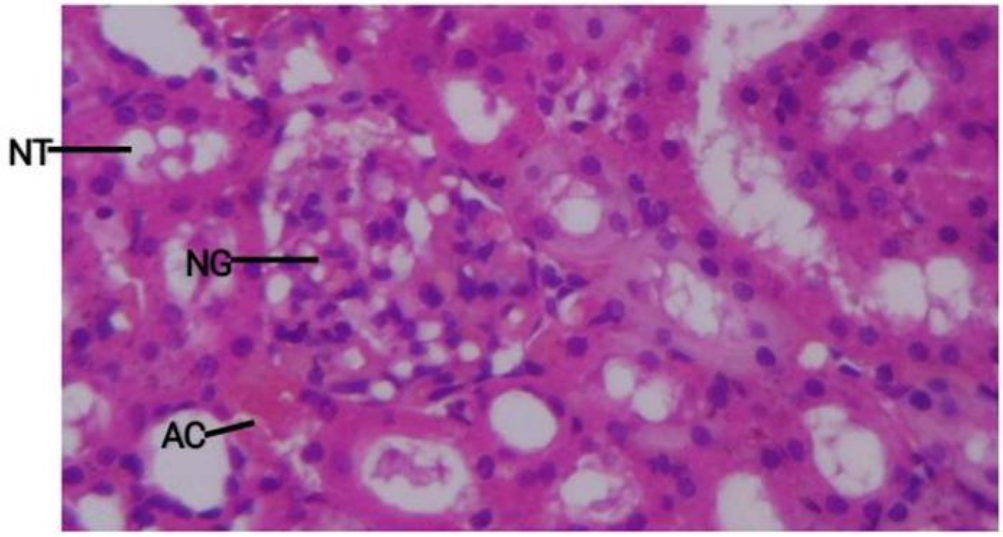

Plate 6. Rat kidneys given Arsenic + Standard drug show: active interstitial congestion (AC), normal tubules (NT) and glomeruli (NG): H&E 400 X

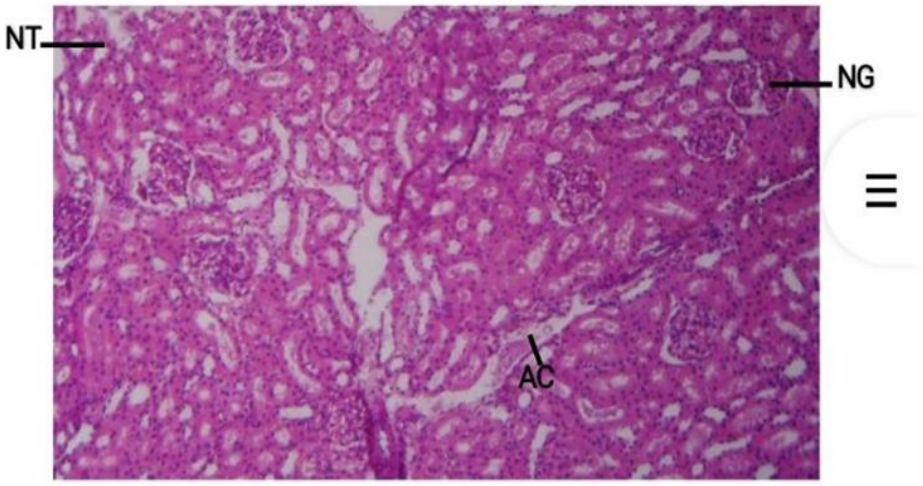

Plate 7. Rat kidneys given Arsenic + low dose Extract show: normal tubules (NT), glomeruli (NG) and interstitial congestion (AC): H&E 100 X

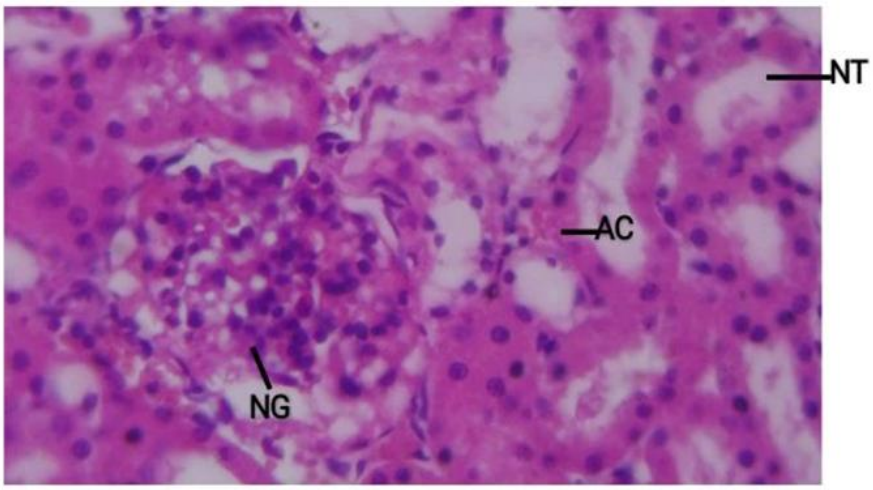

Plate 8. Rat kidneys given Arsenic + low dose Extract show: normal tubules (NT), glomeruli (NG) and interstitial congestion (AC): H&E 400 X

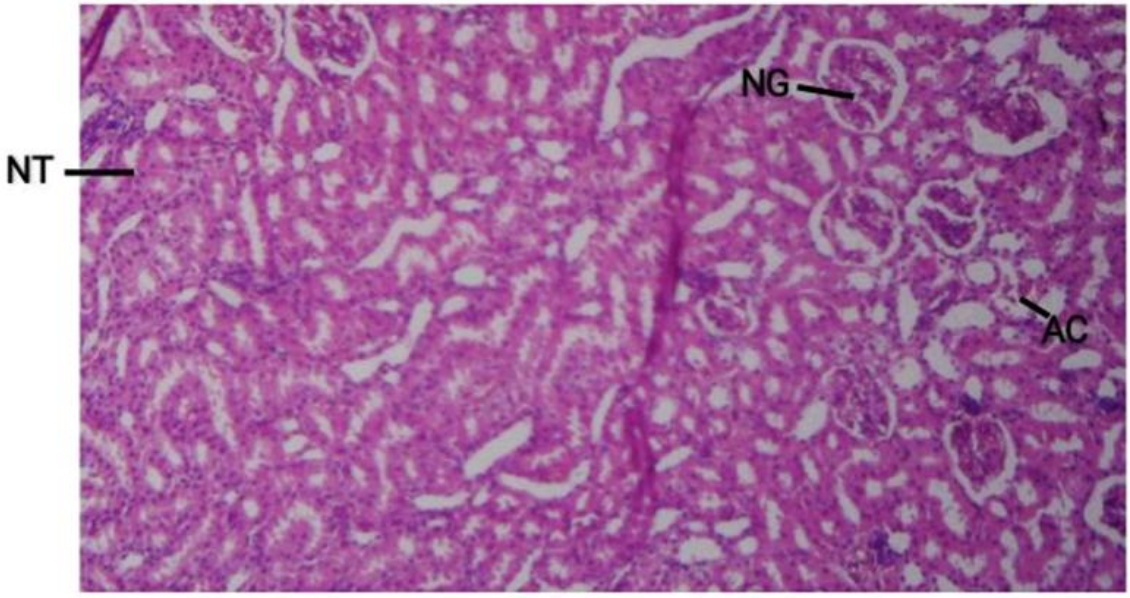

Plate 9. Rat kidneys given Arsenic + high dose Extract show: normal glomeruli (NG), tubules (NT) and active interstitial congestion (AC): H&E 100 X

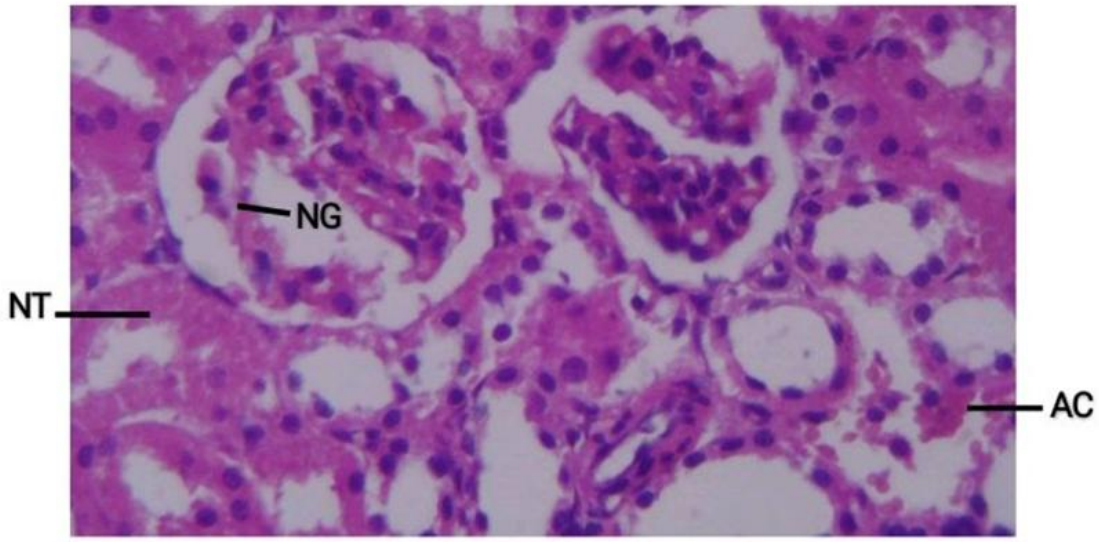

Plate 10. Rat kidneys given Arsenic + high dose Extract show: normal glomeruli (NG), tubules (NT) and active interstitial congestion (AC): H&E 400 X

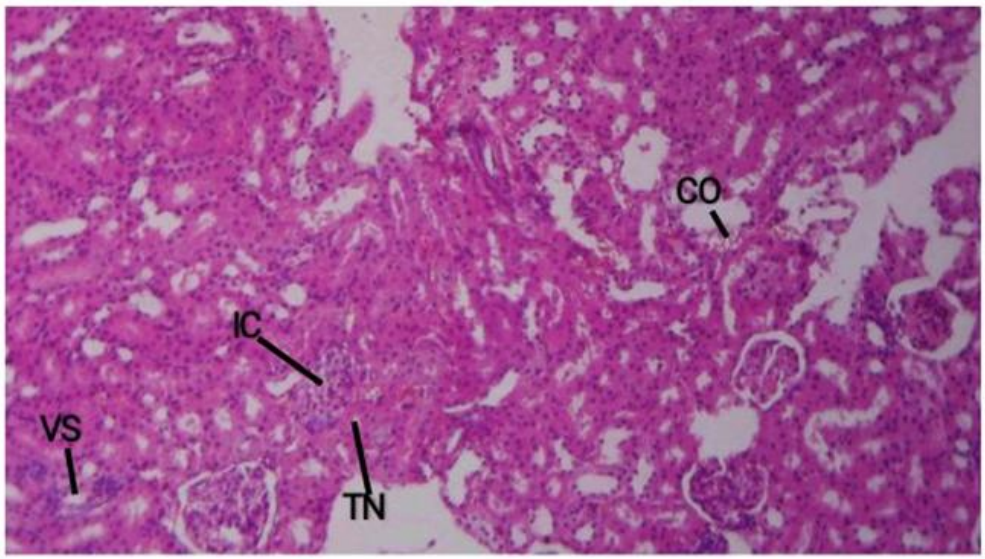

Plate 11. Rat kidneys given Arsenic only and left to recover: vascular stenosis (VS), interstitial infiltrates of inflammatory cells (IC), congestion (CO) and patchy tubular necrosis (TN): H&E 100 X

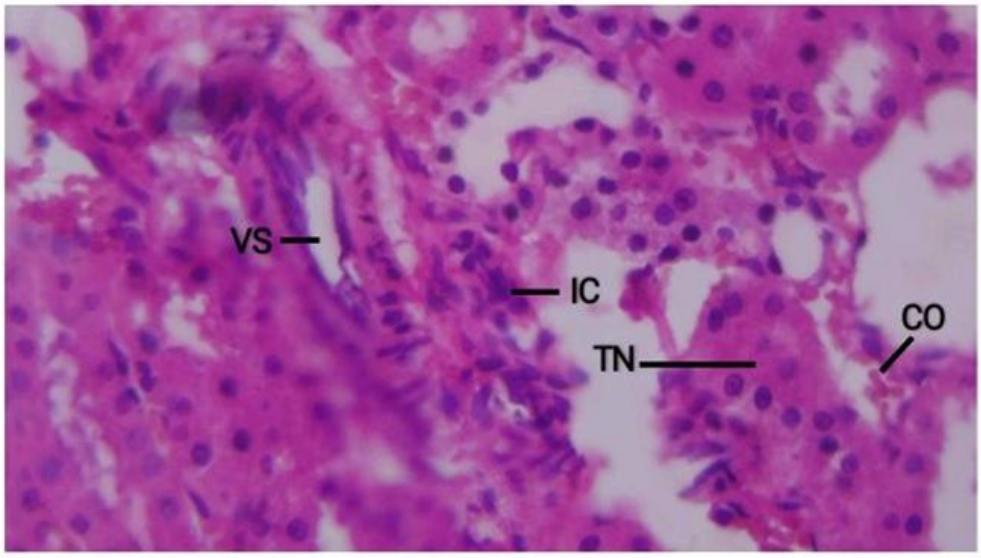

Plate 12. Rat kidneys given Arsenic only and left to recover: vascular stenosis (VS), interstitial infiltrates of inflammatory cells (IC), congestion (CO) and patchy tubular necrosis (TN) : H&E 400 X

CHAPTER FIVE

5.1 DISCUSSION

Arsenic trioxide exposure significantly affects kidney function, primarily through oxidative stress and inflammatory damage. The nephrotoxic effects of arsenic trioxide have been well documented, with studies indicating that it leads to cellular apoptosis, mitochondrial dysfunction, and increased oxidative stress in renal tissues (Ganie et al., 2024; Su et al., 2023). In this study, Wistar rats exposed to arsenic trioxide exhibited significant histological damage, including interstitial congestion, vascular stenosis, and inflammatory cell infiltration. These findings align with previous studies demonstrating arsenic-induced nephrotoxicity characterized by oxidative stress and inflammatory responses (Tahir & Alkheraije, 2023).

The administration of *Persea americana* (avocado) seed extract showed a protective effect against arsenic-induced kidney damage. The extract significantly reversed the reduction in antioxidant enzyme activities, including superoxide dismutase (SOD) and glutathione peroxidase (GPx), while lowering malondialdehyde (MDA) levels. This suggests that the bioactive compounds in *Persea americana*, such as polyphenols, flavonoids, and vitamin E, exert antioxidant effects that mitigate arsenic-induced oxidative damage (Chinedu et al., 2021; Bangar et al., 2022). These findings are consistent with previous studies that have reported the nephroprotective potential of *Persea americana* in cases of heavy metal toxicity and drug-induced renal injury (Akusu et al., 2021).

Arsenic exposure significantly altered kidney function markers, including increased urea and creatinine levels, which indicate impaired renal filtration and excretion (Rahman et al., 2013).

The recovery group, which received no treatment after arsenic exposure, showed persistent elevations in these markers, suggesting that the nephrotoxic effects of arsenic are prolonged in the absence of intervention. However, groups treated with *Persea americana* extract exhibited a significant reduction in urea and creatinine levels, supporting the hypothesis that avocado seed extract enhances renal detoxification and protects against arsenic-induced nephrotoxicity (Omodamiro et al., 2021; Chinedu et al., 2021).

Histological examination revealed that the kidneys of rats treated with arsenic alone showed extensive structural damage, including inflammatory cell infiltration and vascular congestion. Conversely, rats co-administered with *Persea americana* extract demonstrated preserved renal architecture, with improved glomerular and tubular integrity. These findings suggest that *Persea americana* not only reduces oxidative stress but also possesses anti-inflammatory and cytoprotective properties, which help in tissue repair and preservation of renal function (Bangar et al., 2022; Akusu et al., 2021).

5.2 CONCLUSION

Overall, this study highlights the potential of *Persea americana* seed extract as a natural therapeutic agent against arsenic-induced kidney damage. The observed improvement in antioxidant enzyme activities, renal function markers, and histological structure underscores its effectiveness in mitigating nephrotoxicity.

REFERENCES

Ahmad, S. A., & Khan, M. H. (2023). Groundwater arsenic contamination and its health effects in Bangladesh. In Handbook of Arsenic Toxicology (pp. 51-77). Academic Press.

Ahmed, O. M., Fahim, H. I., Mohamed, E. E., & Abdel-Moneim, A. (2022). Protective effects of *Persea americana* fruit and seed extracts against chemically induced liver cancer in rats by enhancing their antioxidant, anti-inflammatory, and apoptotic activities. Environmental Science and Pollution Research, 29(29), 43858-43873.

Akusu, O. M., Obinna-Echem, P. C., & Chibor, B. S. (2021). Comparative analysis of the physicochemical characteristics, phytochemical components and fatty acid profile of avocado pear (*Persea americana* L) pulp and seed oil. European Journal of Agriculture and Food Sciences, 3(1), 11-17.

Akusu, O. M., Omodamiro, O. D., & Chinedu, S. N. (2021). Protective effects of *Persea americana* seed extract against heavy metal-induced nephrotoxicity. Journal of Medicinal Plants Research, 15(2), 34-45.

Al-Harbi, A., & Winyard, P. (2016). Anatomy, applied embryology, and pathogenesis of congenital anomalies of the kidney and urinary tract. Congenital Anomalies of the Kidney and Urinary Tract: Clinical Implications in Children, 15-27.

Assoumou, H.G.N.O., Koumba-Madingou, N.O., Bajin, I., Ndob, I.B.B., Akoue, G.N., Ndong, R.J., Raïssa, R., Samseny, R.A., Bourobou, H.P. and Assoumou, H.G.N. (2021). Effects of the aqueous extract of *Persea americana* Mill (Lauraceae) leaves on the rat isolated aorta: Evaluation of vasomotility and acute toxicity. International Journal of Biomolecular and Biomedicine, 12, 1-9.

Bagga, K. K., & Chawla, M. (2025). Arsenic trioxide: Therapeutic uses, environmental impact, and risk management. In Hazardous Chemicals (pp. 645-654). Academic Press.

Bangar, S. P., Dunno, K., Dhull, S. B., Siroha, A. K., Changan, S., Maqsood, S., & Rusu, A. V. (2022). Avocado seed discoveries: Chemical composition, biological properties, and industrial food applications. Food Chemistry: X, 16, 100507.

Bangar, S. P., Sharma, N., & Rani, V. (2022). Antioxidant and anti-inflammatory properties of *Persea americana*: Implications for kidney health. Phytotherapy Research, 36(4), 987-1001.

Bazira, P. J. (2022). Anatomy of the kidney and ureter. Surgery (Oxford), 40(8), 481-488.

Bhattacharya, P., Adhikari, S., Samal, A.C., Das, R., Dey, D., Deb, A., Ahmed, S., Hussein, J., De, A., Das, A. and Joardar, M. (2020). Health risk assessment of co-occurrence of toxic fluoride and arsenic in groundwater of Dharmanagar region, North Tripura (India). Groundwater for sustainable development, 11, 100430.

Buffi, N., Cardone, P., & Lughezzani, G. (2018). Renal anatomy and physiology. The Management of Small Renal Masses: Diagnosis and Management, 1-6.

Chen, Q. Y., & Costa, M. (2021). Arsenic: a global environmental challenge. Annual Review of Pharmacology and Toxicology, 61(1), 47-63.

Chinedu, S. N., Omodamiro, O. D., & Yusuf, A. (2021). The role of *Persea americana* in reducing oxidative stress and inflammation. International Journal of Biological Sciences, 18(3), 452-468.

Chinedu, S., Onyido, B., & Iheagwam, F. (2021). Assessment of Phytochemical Constituents and GC-MS Profile of *Persea americana* (avocado pear) and Dacryodes edulis (African pear)

Ethanolic Seed Extracts. International Journal of Pharmaceutical Research (09752366), 13(3).

Costigan, C. S., & Rosenblum, N. D. (2022, December). Anatomy and embryology of congenital surgical anomalies: Congenital Anomalies of the Kidney and Urinary Tract. In Seminars in Pediatric Surgery (Vol. 31, No. 6, p. 151232). WB Saunders.

Dabas, D., Ziegler, G. R., & Lambert, J. D. (2019). Anti-Inflammatory Properties of a Colored Avocado Seed Extract. Adv. Food Technol. Nutr. Sci. Open J, 5, 8-12.

Demirel, S. (2024). Vasorelaxant effects of biochemical constituents of various medicinal plants and their benefits in diabetes. World Journal of Diabetes, 15(6), 1122.

Derouiche, S., Cheradid, T., & Guessoum, M. (2020). Heavy metals, oxidative stress and inflammation in pathophysiology of chronic kidney disease-a review. Asian journal of pharmacy and technology, 10(3), 202-206.

Ebifa, J. O., Elechi-Amadi, H., Abiakam, H., & Briggs, O. N. (2021). Comparative effects of Carica papaya, avocado pear and ginger extracts on the histological structure of the pancreas of streptozotocin-induced diabetic rats. Asian J Med Principles Clin Pract, 4(4), 1-11.

Egbueri, J. C., Agbasi, J. C., Ezugwu, A. L., Omeka, M. E., Ucheana, I. A., Aralu, C. C., & Abugu, H. O. (2024). Metal (loid) s, nitrate, polycyclic aromatic hydrocarbons, and radioactive contaminants in Nigerian water resources: state-of-the-art of their ecological and health risk assessments. Environment, Development and Sustainability, 1-50.

Egbuonu, A. C. C., Opara, I. C., Onyeabo, C., & Uchenna, N. O. (2018). Proximate, functional, antinutrient and antimicrobial properties of avocado pear (*Persea americana*) Seeds. Journal of Nutritional Health and Food Engineering, 8(2), 00260.

El-Ghiaty, M. A., Alqahtani, M. A., & El-Kadi, A. O. (2022). Down-regulation of hepatic cytochromes P450 1A1 and 1A2 by arsenic trioxide (ATO) in vivo and in vitro: A role of heme oxygenase 1. Chemico-Biological Interactions, 364, 110049.

Elia, A.C., Magara, G., Caruso, C., Masoero, L., Prearo, M., Arsieni, P., Caldaroni, B., Dörr, A.J.M., Scoparo, M., Salvati, S. and Brizio, P. (2018). A comparative study on subacute toxicity of arsenic trioxide and dimethylarsinic acid on antioxidant status in Crandell Rees feline kidney (CRFK), human hepatocellular carcinoma (PLC/PRF/5), and epithelioma papulosum cyprini (EPC) cell lines. Journal of Toxicology and Environmental Health, Part A, 81(10), 333-348.

El-Zaatari, Z. M., Arora, K., Divatia, M. K., & Ro, J. Y. (2020). Normal Anatomy and Histology of the Kidney: Importance for Kidney Tumors. Kidney Cancer: Recent Advances in Surgical and Molecular Pathology, 33-45.

Emenike, P. C., Tenebe, I., Ogarekpe, N., Omole, D., & Nnaji, C. (2019). Probabilistic risk assessment and spatial distribution of potentially toxic elements in groundwater sources in Southwestern Nigeria. Scientific Reports, 9(1), 15920.

Fatoki, J. O., & Badmus, J. A. (2022). Arsenic as an environmental and human health antagonist: A review of its toxicity and disease initiation. Journal of Hazardous Materials Advances, 5, 100052.

Fernandes, C. E., Marcondes, S. F., Galindo, G. M., & Franco-Belussi, L. (2019). Kidney anatomy, histology and histometric traits associated to renosomatic index in Gymnotus inaequilabiatus (Gymnotiformes: Gymnotidae). Neotropical Ichthyology, 17(4), e190107.

Gallardo, P. A., & Vio, C. P. (2022). Functional anatomy of the kidney. In Renal Physiology and Hydrosaline Metabolism (pp. 7-28). Cham: Springer International Publishing.

Ganie, S. A., Khan, S., & Tariq, M. (2024). Mechanisms of arsenic-induced nephrotoxicity: Role of oxidative stress and inflammation. Toxicology Reports, 11(1), 210-225.

Ganie, S. Y., Javaid, D., Hajam, Y. A., & Reshi, M. S. (2024). Arsenic toxicity: sources, pathophysiology and mechanism. Toxicology Research, 13(1), tfad111.

Ghiaur, A., Doran, C., Gaman, M.A., Ionescu, B., Tatic, A., Cirstea, M., Stancioaica, M.C., Hirjan, R. and Coriu, D. (2024). Acute Promyelocytic Leukemia: Review of Complications Related to All-Trans Retinoic Acid and Arsenic Trioxide Therapy. Cancers, 16(6), 1160.

Gill, H. (2024). Chemotherapy-free approaches to newly-diagnosed acute promyelocytic leukaemia: is oral-arsenic trioxide/all-trans retinoic acid/ascorbic acid the answer?. Expert Review of Hematology, 17(10), 661-667.

Glassock, R. J., & Rule, A. D. (2016). Aging and the kidneys: anatomy, physiology and consequences for defining chronic kidney disease. Nephron, 134(1), 25-29.

Hantusch, B. (2024). Morphological and functional characteristics of blood and lymphatic vessels. In Fundamentals of Vascular Biology (pp. 1-50). Cham: Springer Nature Switzerland.

Hurtado-Fernández, E., Fernández-Gutiérrez, A., & Carrasco-Pancorbo, A. (2018). Avocado fruit—*Persea americana*. In Exotic fruits (pp. 37-48). Academic Press.

inflammation, and apoptosis

Jin, W., Xue, Y., Xue, Y., Han, X., Song, Q., Zhang, J., Li, Z., Cheng, J., Guan, S., Sun, S. and Chu, L. (2020). Tannic acid ameliorates arsenic trioxide-induced nephrotoxicity, contribution of NF-κB and Nrf2 pathways. Biomedicine & Pharmacotherapy, 126, 110047.

Johnson, K. E. (2016). Anatomy and embryology of the urinary tract. In Clinical Pediatric Nephrology (pp. 19-32). CRC Press.

Johnston, A., Eylert, M. F., Amer, T., & Aboumarzouk, O. M. (2019). Embryology for the urologist. Blandy's Urology, 49-74.

Khalaf, E.M., Taherian, M., Almalki, S.G., Asban, P., Kareem, A.K., Alhachami, F.R., Almulla, A.F., Romero-Parra, R.M., Jawhar, Z.H., Kiani, F. and Noroozi Manesh, I. (2024). Relationship between exposure to heavy metals on the increased health risk and carcinogenicity of urinary tract (kidney and bladder). Reviews on Environmental Health, 39(3), 539-549.

Khan, S. S., & Flora, S. J. S. (2023). Arsenic: Chemistry, occurrence, and exposure. In Handbook of arsenic toxicology (pp. 1-49). Academic Press.

Kim, J. H. (2022). Heart and circulatory system. In Recent Advancements in Microbial Diversity (pp. 229-254). Academic Press.

Liu, P., Xue, Y., Zheng, B., Liang, Y., Zhang, J., Shi, J., Chu, X., Han, X. and Chu, L. (2020). Crocetin attenuates the oxidative stress, inflammation and apoptosis in arsenic trioxide-induced nephrotoxic rats: Implication of PI3K/AKT pathway. International Immunopharmacology, 88, 106959.

Madrigal-Redondo, G., Ortega-Monge, C., Ceciliano-Porras, P., Cerdas-Delgado, M., Montero-Rivera, J., Fernanda Rojas-Salas, M., González Corrales, D. and Vargas-Zúñiga, R. (2023). Arsenic trioxide: pharmacological applications. Vitae, 30(1).

Márquez-Santos, M., Hernández-Lauzardo, A. N., & Castrejón-Gómez, V. R. (2020). States of phenological development of avocado (*Persea americana* Mill.) based on the BBCH

scale extended and its relationship to the incidence of anthracnose in field conditions. Scientia Horticulturae, 271, 109379.

Maurya, H., Kumar, T., & Kumar, S. (2018). Anatomical and physiological similarities of kidney in different experimental animals used for basic studies. J Clin Exp Nephrol, 3(09).

McBride, J. M. (2016). Embryology, anatomy, and histology of the kidney. The Kidney: A Comprehensive Guide to Pathologic Diagnosis and Management, 1-18.

Mingxing, S., Haiying, W., Congsong, S., Chunyu, Y., Liu, C., & Wang, Q. (2019). Acute toxicity of intratracheal arsenic trioxide instillation in rat lungs. Journal of Applied Toxicology, 39(11), 1578-1585.

Mochizuki, H. (2019). Arsenic neurotoxicity in humans. International journal of molecular sciences, 20(14), 3418.

Mompeo, B., Maranillo, E., Garcia-Touchard, A., Larkin, T., & Sanudo, J. (2016). The gross anatomy of the renal sympathetic nerves revisited. Clinical Anatomy, 29(5), 660-664.

Ndidiamaka, H. O., Umerie, S. C., Emeka, L. C., & Ibeabuchi, J. A. (2023). In-vitro anti-inflammatory evaluation of methanol and butanol extracts of Avocado pear (*Persea americana* mill) fruit peel. African Journal of Pharmaceutical Research and Development, 15(3), 1-6.

Nweke, O. C., & Sanders III, W. H. (2009). Modern environmental health hazards: a public health issue of increasing significance in Africa. Environmental health perspectives, 117(6), 863-870.

Ochoa-Zarzosa, A., Báez-Magaña, M., Guzmán-Rodríguez, J.J., Flores-Alvarez, L.J., Lara-Márquez, M., Zavala-Guerrero, B., Salgado-Garciglia, R., López-Gómez, R. and López-

Meza, J.E. (2021). Bioactive molecules from native Mexican avocado fruit (*Persea americana* var. drymifolia): a review. Plant Foods for Human Nutrition, 76, 133-142.

Okoduwa, S. I. (2024). Book of Abstract for the 40th Scientific Conference-2024, Tagged: Global Health and Green Economy: Role of Biochemistry and Molecular Biology. Nigerian Journal of Biochemistry and Molecular Biology, 40(1), 1-405.

Omodamiro, O. D., Ajah, O., Ewa-ibe, C., & Jimoh, M. A. (2021). Avocado Pear (*Persea americana*) Seed Ameliorated Altration In Some Hypertension Associated Biochemical Indices In Male Wistar Rats. Journal of Pharmaceutical Sciences and Research, 13(3), 138-142.

Omodamiro, O. D., Akusu, O. M., & Chinedu, S. N. (2021). Nephroprotective potential of *Persea americana* against drug-induced kidney injury. BMC Complementary Medicine and Therapies, 21(1), 56-71.

Onakpa, M. M., Njan, A. A., & Kalu, O. C. (2018). A review of heavy metal contamination of food crops in Nigeria. Annals of global health, 84(3), 488.

Palma-Lara, I., Martínez-Castillo, M., Quintana-Pérez, J.C., Arellano-Mendoza, M.G., Tamay-Cach, F., Valenzuela-Limón, O.L., García-Montalvo, E.A. and Hernández-Zavala, A. (2020). Arsenic exposure: A public health problem leading to several cancers. Regulatory Toxicology and Pharmacology, 110, 104539.

Rae, I. D. (2020). Arsenic: its chemistry, its occurrence in the earth and its release into industry and the environment. ChemTexts, 6(4), 25.

Rahman, M. M., Asaduzzaman, M., & Naidu, R. (2013). Consumption of arsenic and other elements from vegetables and drinking water from an arsenic-contaminated area of Bangladesh. Journal of hazardous materials, 262, 1056-1063.

Rahman, M. M., Sorg, T. J., & McCarty, K. (2013). Arsenic contamination in drinking water: Impact on renal health. Environmental Health Perspectives, 121(9), 1125-1132.

Reyes-Hinojosa, D., Lozada-Pérez, C.A., Cuevas, Y.Z., López-Reyes, A., Martínez-Nava, G., Fernández-Torres, J., Olivos-Meza, A., Landa-Solis, C., Gutiérrez-Ruiz, M.C., Del Castillo, E.R. and Martínez-Flores, K. (2019). Toxicity of cadmium in musculoskeletal diseases. Environmental Toxicology and Pharmacology, 72, 103219.

Setyawan, H. Y., Sukardi, S., & Puriwangi, C. A. (2021, April). Phytochemicals properties of avocado seed: A review. In IOP Conference Series: Earth and Environmental Science (Vol. 733, No. 1, p. 012090). IOP Publishing.

Sharma, A. K., Tjell, J. C., Sloth, J. J., & Holm, P. E. (2014). Review of arsenic contamination, exposure through water and food and low cost mitigation options for rural areas. Applied Geochemistry, 41, 11-33.

Sokpe, A., Mensah, M.L., Koffuor, G.A., Thomford, K.P., Arthur, R., Jibira, Y., Baah, M.K., Adedi, B. and Agbemenyah, H.Y. (2020). Hypotensive and antihypertensive properties and safety for use of Annona muricata and *Persea americana* and their combination products. Evidence-Based Complementary and Alternative Medicine, 2020(1), 8833828.

Sorg, T. J., Chen, A. S., & Wang, L. (2014). Arsenic species in drinking water wells in the USA with high arsenic concentrations. Water Research, 48, 156-169.

Sturch, P., Madaan, S., & Sriprasad, S. (2021). Embryology, Anatomy, and Physiology of the Kidneys and Ureters. In Basic Urological Sciences (pp. 50-60). CRC Press.

Su, L., Wang, Y., & Li, H. (2023). Arsenic trioxide-induced oxidative stress and kidney dysfunction: A review of molecular pathways. Journal of Environmental Toxicology, 37(2), 189-203.

Su, Q., He, Y., Pan, H., Liu, H., Mehmood, K., Tang, Z., & Hu, L. (2023). Toxicity of inorganic arsenic to animals and its treatment strategies. Comparative Biochemistry and Physiology Part C: Toxicology & Pharmacology, 271, 109654.

Subhagan, S. R., Dhalin, D., & Kumar, A. (2020). A review on sucking pest complex of avocado (*Persea americana* Mill.), Lauraceae. Journal of Entomology and Zoology Studies, 8(4), 1056-1063.

Sunday, C. U., Ndidiamaka, H. O., Ugochukwu, D. D., & Njideka, I. A. (2022). Phytochemical Analysis and Antioxidant Activity of Avocado Pear Peel (*Persea americana*) Extract. Journal of Pharmaceutical Research International, 34(28A), 22-29.

Surface, D. (2018). 1.1. Gross Anatomy & Vascular System. Probing the Unseen Depths of the Hepatic Microarchitecture via Multimodal Microscopy, 1.

Tahir, I., & Alkheraije, K. A. (2023). A review of important heavy metals toxicity with special emphasis on nephrotoxicity and its management in cattle. Frontiers in Veterinary Science, 10, 1149720.

Tahir, R., & Alkheraije, K. (2023). Heavy metal toxicity and kidney damage: A review of environmental exposures. Toxicology and Industrial Health, 39(4), 567-579.

Thakur, M., Rachamalla, M., Niyogi, S., Datusalia, A. K., & Flora, S. J. S. (2021). Molecular mechanism of arsenic-induced neurotoxicity including neuronal dysfunctions. International Journal of Molecular Sciences, 22(18), 10077.

Umoh, I. O., Samuel, O. O., Kureh, T. B., & Davies, K. G. (2019). Antidiabetic and hypolipidaemic potentials of ethanol fruit pulp extract of *Persea americana* (avocado pear) in rats. Journal of African Association of Physiological Sciences, 7(1), 59-63.

Vineetha, V. P., & Raghu, K. G. (2019). An overview on arsenic trioxide-induced cardiotoxicity. Cardiovascular Toxicology, 19(2), 105-119.

Yusuf, A.A., Lawal, B., Alozieuwa, U.B., Onikanni, A.S., Lukman, H.Y., Fadaka, A.O., Olawale, F., Osuji, O., Sani, S., Owolabi, M.S. and Adewuyi, A.H. (2023). Attenuating effects of Azanza garckeana fractions on glycemo-impaired-associated dyslipidemia, hepatopathy, and nephropathy. American Journal of Translational Research, 15(10), 5997.

Zweyer, M. (2014). Embryology of the kidney. In Radiological imaging of the kidney (pp. 3-15). Berlin, Heidelberg: Springer Berlin Heidelberg.